Full Length Article

Clayey soil stabilization using alkali-activated volcanic ash and slag

Hania Miraki [a], Nader Shariatmadari [a], Pooria Ghadir [a], Soheil Jahandari [b,*], Zhong Tao [b], Rafat Siddique [c]

[a] Department of Civil Engineering, Iran University of Science and Technology, Tehran, Iran
[b] Centre for Infrastructure Engineering, Western Sydney University, Penrith, NSW, 2751, Australia
[c] Thapar Institute of Engineering and Technology, Patiala, India

ARTICLE INFO

ABSTRACT

Lime and Portland cement are the most widely used binders in soil stabilization projects. However, due to the high carbon emission in cement production, research on soil stabilization by the use of more environmentally-friendly binders with lower carbon footprint has attracted much attention in recent years. This research investigated the potential of using alkali-activated ground granulated blast furnace slag (GGBS) and volcanic ash (VA) as green binders in clayey soil stabilization projects, which has not been studied before. The effects of different combinations of VA with GGBS, various liquid/solid ratios, different curing conditions, and different curing periods (i.e. 7 d, 28 d and 90 d) were investigated. Compressive strength and durability of specimens against wet-dry and freeze-thaw cycles were then studied through the use of mechanical and microstructural tests. The results demonstrated that the coexistence of GGBS and VA in geopolymerization process was more effective due to the synergic formation of N-A-S-H and C-(A)-S-H gels. Moreover, although VA needs heat curing to become activated and develop strength, its partial replacement with GGBS made the binder suitable for application at ambient temperature and resulted in a remarkably superior resistance against wet-dry and freeze-thaw cycles. The carbon embodied of the mixtures was also evaluated, and the results confirmed the low carbon footprints of the alkali-activated mixtures. Finally, it was concluded that the alkali-activated GGBS/VA could be promisingly used in clayey soil stabilization projects instead of conventional binders.

1. Introduction

The undesirable properties associated with soft soils, such as poor shear strength and high compressibility, make it necessary for engineers to adopt a proper stabilization method to meet the required engineering properties (Ghasemi et al., 2019; Saberian et al., 2020). The most common and conventional method for soft soil improvement is chemical stabilization in which lime and Portland cement are the most widely utilized binders (Jahandari et al., 2017a,b; Saberian et al., 2017a, 2018; Bahmani et al., 2019; Farhangi et al., 2020; Kazemi et al., 2020a,b). Strength development in these methods is provided through the pozzolanic reactions and hydration, which are well-known reactions among calcium hydroxide alumina and/or silica and water. The final products of these reactions depend on the content of the available silica and alumina, which can be calcium aluminate hydrate, calcium silicate hydrate and calcium aluminoslica hydrate (Dodson, 1990).

Cement is the most common binder used in the road and construction industry, and the annual production rate of cement is increasing at a ground-breaking pace. In 2015, cement manufacturers produced 4.6 billion tons worldwide (Scrivener et al., 2018). It is estimated that this amount will reach 4.83 billion tons by 2030 (Scrivener et al., 2018; Gopalakrishnan and Chinnaraju, 2019). This amount of production is responsible for plenty of adverse environmental impacts, for instance, manufacturing 1 ton cement and 1 ton lime accounts for 0.95 and 0.79 tons of CO_2 emission (about 5%–8% global anthropogenic CO_2 emission) and also consumes 5000 MJ and 3200 MJ energy, respectively (Shand, 2006; Higgins, 2007; Lemougna et al., 2017a, 2018). Moreover, cement production accelerates the depletion of natural resources, and results in the consumption of about 1.5 ton limestone and clay per each ton of cement (McLellan et al., 2011). Apart from the environmental issues, Portland cement has some other drawbacks such as

mechanical strength reduction due to the loss of water, unfinished hydration at the beginning stages and high plastic shrinkage, which are of special importance for geotechnical engineering applications, particularly in torrid zones (Bushlaibi and Alshamsi, 2002; Ghadir and Ranjbar, 2018).

The above-mentioned drawbacks have motivated researchers to investigate the possibility of using environmentally-friendly materials as an alternative for conventional binders (Mehrabi et al., 2021). Geopolymers, known as the new generation of green materials for cement substitution, are synthesized from the chemical reaction between an amorphous precursor, which is rich in alumina (Al_2O_3) and silicate (SiO_2) with a sodium or potassium-based activator (Provis and Bernal, 2014). Briefly, the geopolymerization process includes two main steps: first, dissolution of aluminosilicate oxides in the alkali activator and second, poly-condensation accomplished through diffusion of the tetrahedral units of $[SiO_4]^-$ and $[AlO_4]^-$ and their reaction with alkali activator which finally results in the formation of a sodium aluminosilicate gel (Xu and Van Deventer, 2002; Komnitsas and Zaharaki, 2007). The most widely used activators for the activation of precursors in geopolymers are sodium hydroxide (NaOH), sodium silicate (Na_2SiO_3), or a mixture of them (Turner and Collins, 2013). However, using sodium silicate has some adverse environmental impacts since the production of 1 ton sodium silicate releases 1.514 ton CO_2 (Turner and Collins, 2013). Although CO_2 embodied of some of the activators such as sodium silicate is higher than that of Portland cement, the amount of alkaline solution used to produce geopolymer is remarkably lower than that of Portland cement utilized in conventional binders which leads to a lower CO_2 emission.

Geopolymer is mainly referred to the alkali-activated products with a high content of aluminosilicate and low content of calcium (Provis and Van Deventer, 2013). However, in the current research, ground granulated blast furnace slag (GGBS) with high calcium content was employed in the mixtures; therefore, it is more reasonable to use the term alkali-activated material (AAM) instead of geopolymer. AAM is the broadest term to designate any binder system resulting from the reaction between an alkali metal source (solid or dissolved) with a solid silicate powder (Buchwald et al., 2003). In contrast, geopolymers (Davidovits, 1991) are in many cases viewed as a subset of AAMs, where the binding phase is almost exclusively aluminosilicate and highly coordinated. For the formation of such a gel as the principal binding phase, the available calcium content of the reacting components should commonly be low to enable formation of a pseudo-zeolitic network structure rather than the chains characteristic of calcium silicate hydrates (Provis et al., 2005). In addition to calcium silicate hydrates, aluminosilicate hydrates may be formed in the structure of AAMs with a mostly Q3 structure, while geopolymers have a three-dimensional (3D) Q4 structure.

Currently, due to the promising properties of AAMs such as low carbon footprint (Provis and Van Deventer, 2013; Ghadir et al., 2021a), high compressive strength (Du et al., 2016), excellent resistance to fire and acid (Gao et al., 2013; Rios et al., 2019; Shariatmadari et al., 2021), rapid strength development (Phoongernkham et al., 2016), desirable ductility (Zhang et al., 2013), and low shrinkage (Nath and Sarker, 2017), increasing attention is being paid to the use of these materials.

There are several waste materials such as volcanic ash (VA), fly ash and rice husk ash, which have the potential to be utilized as the precursor for AAM synthesis. Since there is no need for VA to be combusted before using, it is considered as one of the most desirable materials among the natural aluminosilicates (Lemougna et al., 2011; Takeda et al., 2014). However, the practical application of VA in soil stabilization projects has been quite limited since hardening of their slurry in a conventional time to gain desirable compressive

strength requires the curing temperature of 50 °C–100 °C (Lemougna et al., 2011; Takeda et al., 2014; Djobo et al., 2017). Although this may not be considered as a high temperature, applying this temperature in the field is not practically feasible nor energy-efficient. On the other hand, there are some aluminosilicate materials such as GGBS for AAM synthesis, which can provide desirable reactivity at ambient temperature. GGBS is a by-product of the steel manufacturing process, and it is mostly landfilled in large amounts. In the process of generating 1 ton GGBS, only 1300 MJ energy is consumed, and 0.07 ton of CO_2 is released, which are comparatively lower than those generated in the production of cement (Higgins, 2007). In the reaction process of GGBS, the liquid alkali activator breaks Si–O and Al–O bonds in GGBS resulting in strength development and stabilization of the soil by the formation of calcium silicate hydrate (C–S–H), calcium aluminate hydrate (C-A-H), and calcium aluminate silicate hydrate (C-A-S-H) gels (Wang and Scrivener, 1995; Chew et al., 2004).

The mechanical properties of AAMs depend on several factors such as the properties and content of the precursor, chemical composition and content of the alkali activator, liquid/solid ratio, curing time and curing temperature. It has been reported that increasing the amount of precursors such as fly ash, GGBS and metakaolin leads to higher compressive strengths (Xu and Van Deventer, 2002; Singhi et al., 2016). In a research on fly ash, palm oil fuel ash and kaolin-based geopolymers, increasing the content of alkali activator in the mixture up to a specific content resulted in compressive strength development due to the more dissolution of aluminium and silicon in the mixture (Heah et al., 2012; Suksiripattanapong et al., 2015; Phetchuay et al., 2016; Sukmak et al., 2019; Yaghoubi et al., 2019). In a comparison between a soil treated with lightweight alkali-activated GGBS and the same soil treated with lightweight-Portland cement (OPC), it is reported that the mechanical performance of the former was increased by 200%–350% compared to the latter (Du et al., 2017). Similarly, by utilizing the same percentage of binder, after a curing period of 28 d, the alkali-activated GGBS stabilized soil was observed to have a 600% enhancement in its compressive strength compared with OPC-stabilized soil (Singhi et al., 2017). Furthermore, increasing the ratio of activator/binder, for instance, Na_2O/fly ash from 0.16 to 0.375, resulted in a 50% reduction in the compressive strength. The diversities in the results could be related to the different chemical compositions of the components and different curing times and conditions (Cristelo et al., 2013a). In another research, the effects of different types of activators on the uniaxial compressive strength (UCS) of stabilized soil by alkali-activated GGBS were studied, and the results were compared with that of OPC-stabilized soil. The results of this research indicated that among all of the utilized activators, NaOH provided the highest UCS values after 7 d, 28 d and 90 d of curing; however, a reduction in the strength of the stabilized clay was observed from 90 d to 180 d. Moreover, among the specimens prepared by different types of activators, fewer-large sized pores were observed for the samples activated by NaOH (Yi et al., 2015). The potential of using VA-based geopolymer for clayey soil stabilization at different curing conditions was investigated in a research, and the results showed that incorporating 15% VA increased the UCS values from 0.2 MPa to 4 MPa and 2 MPa to 12 MPa in wet and dry conditions, respectively (Ghadir and Ranjbar, 2018). In another research carried out to investigate the geopolymerization of VA blended with GGBS, it is reported that GGBS contribution in geopolymerization resulted in a reduction in setting time from 7 d to a couple of hours and an increase in the UCS up to 85 MPa (Lemougna et al., 2020). A recent research on geopolymer synthesized from the mixture of fly ash and slag for marine clay stabilization showed that an increase in the binder content led to higher UCS values. Additionally, increasing the activator/binder

ratio from 0.75 to 1 resulted in an increase in the UCS; however, increasing this ratio from 1 to 1.25 led to a decrease in UCS values (Yaghoubi et al., 2019).

A glance at the above-mentioned literature indicates that there is limited research on the application of AAMs in soil stabilization. For stabilization of clayey soil, providing an adequate amount of calcium is the most important concern for the stabilizer (Wang, 2002). Since VA is relatively rich in silica and alumina but deficient in calcium oxide and GGBS is rich in calcium oxide, the coexistence of these two materials could be more effective due to the synergic formation of N-A-S-H and C-(A)-S-H gels. It has been previously reported that VA requires a temperature of 50 °C–100 °C to become activated (Takeda et al., 2014; Djobo et al., 2017), whereas GGBS has a desirable reactivity at ambient temperature. Hence, utilizing a mixture of these two materials enables them to be applicable in wider ranges of temperatures. Additionally, the use of VA and GGBS in soil stabilization projects would mitigate the necessity of broadening the currently existing landfills or the need for creating new landfills.

Literature review demonstrates that the focus of the previous studies in the field of soil stabilization using geopolymers and AAMs has mainly been on investigating the mechanical properties (Verdolotti et al., 2008; Cristelo et al., 2011; Cristelo et al., 2013a,b; Liu et al., 2016; Phummiphan et al., 2016; Singhi et al., 2017). However, the long-term performance of these materials such as their durability under freeze-thaw (F-T) and wet-dry (W-D) cycles has not been studied, which restricts the broad application of AAMs in soil stabilization projects. Moreover, although in mortar, brick, ceramic and concrete manufacturing, the conditions of production are often thoroughly controllable, in soil stabilization projects, conditions could be variable. For example, in Kerman city in Iran, the air and ground temperatures fluctuate between −15 °C and 65 °C during summers and winters, respectively, leading to freezing and thawing in the materials (Saberian et al., 2017b). Besides, in some ground improvement projects such as deep soil mixing, some parameters like liquid/solid ratio might be variable in the field.

Based on the above research background, this research was carried out to comprehensively evaluate the feasibility of using alkali-activated VA/GGBS in clayey soil stabilization from different angles. The impacts of different parameters such as different percentages of VA replaced by GGBS, liquid/solid ratio (L/S), curing temperature, and curing time were investigated. Compressive strength, F-T and W-D durability tests were performed to study the mechanical and durability properties of the stabilized soil. X-ray diffraction (XRD), Fourier transform infrared spectroscopy (FTIR), field emission scanning electron microscopy (FESEM), energy dispersive X-ray spectroscopy (EDS) and elemental mapping were also used to comprehensively study the microstructural properties of the stabilized soil. At last but not least, the carbon embodied of the stabilized soil was calculated and reported.

2. Properties of materials

The clayey soil used in this research was sourced from Mazandaran Province, Iran. The liquid limit (*LL*), plastic limit (*PL*), and plasticity index (*PI*) of the soil were measured as 29%, 19% and 10%, respectively, following ASTM D424-54 (1982) and ASTM D423-66 (1972). Sieve analysis and hydrometer tests were also performed according to ASTM D422-63 (2002) and ASTM D7928-17 (2017), respectively and the grain size distribution curve was drawn (Fig. 1). According to the results, the soil is classified as clayey soil with low plasticity (CL) based on ASTM 2487-11 (2011). The optimum water content and maximum dry density of the soil were 13.76% and 1.95 g/cm^3, respectively, obtained through modified Proctor compaction test following ASTM D1557-09 (2009). The VA
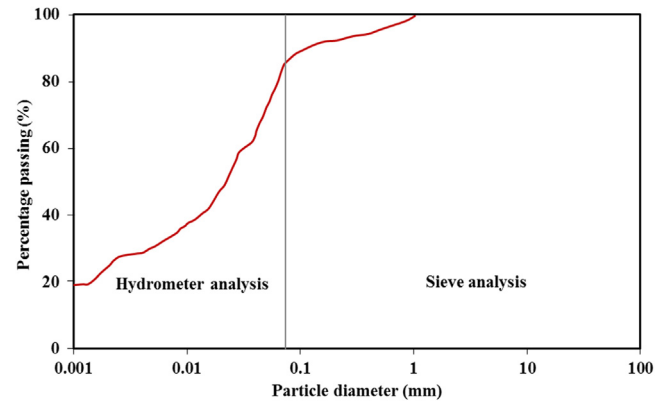

Fig. 1. Grain size distribution curve of the tested soil.

and GGBS used were respectively obtained from the Taftan Mountain, located in the southeast of Iran, and Isfahan Steel Plant located in Isfahan Province, Iran. The chemical compositions of VA, GGBS and soil obtained through the X-ray fluorescence (XRF) test are presented in Table 1. The results show that VA is relatively rich in silica and alumina but deficient in calcium oxide while GGBS is rich in calcium oxide, as previously mentioned for stabilization of clayey soil, providing an adequate amount of calcium is the most important concern for the stabilizer (Wang, 2002).

Fig. 2 shows the FESEM micrograph of the soil with its EDS analysis. EDS analysis was conducted on the yellow square shown in Fig. 2. As can be seen, the soil particles have different sizes and irregular geometric shapes with a relatively dense surface. Oxygen, silicon, calcium, aluminum and magnesium, detected in EDS analysis, were the main compositions of the soil.

Fig. 3 shows the FESEM micrographs of VA and GGBS, both of which composed of particles with different sizes and irregular geometric shapes; however, GGBS has more porosity compared with VA.

The used liquid alkali activator was sodium hydroxide with a concentration of 6 M. The proper concentration for NaOH has been reported to be generally between 4.5 and 18 M (Andini et al., 2008; Rattanasak and Chindaprasirt, 2009; Somna et al., 2011; Hanjitsuwan et al., 2014). Since being environmental-friendly and cost-effective were of special importance in this research, a low concentration of 6 M was considered in all mixes. To avoid fast setting, previous studies suggested cooling NaOH solution for 24 h prior to use (Ismail et al., 2014; Bilondi et al., 2018). This practice

Table 1
Chemical composition of the materials used.

Component oxide	Content (wt%)		
	Soil	VA	GGBS
CaO	15	10.1	33.2
SiO$_2$	43.3	54.9	36.1
Al$_2$O$_3$	16.1	20.8	14.4
Fe$_2$O$_3$	6.3	3.3	0.3
MgO	3.8	1.8	6.8
Na$_2$O	1.3	5.8	1.3
K$_2$O	2.3	1.8	1
P$_2$O$_5$	N.D.	0.2	N.D.
TiO$_2$	0.6	0.5	1.6
SO$_3$	0	0.7	3.4
Sr	N.D.	0.1	0.6
Ba	N.D.	N.D.	0.2
MnO	0.1	0	1
LOI	11.2	0.1	0.1

Note: N.D. represents none detected.

(a)   (b)
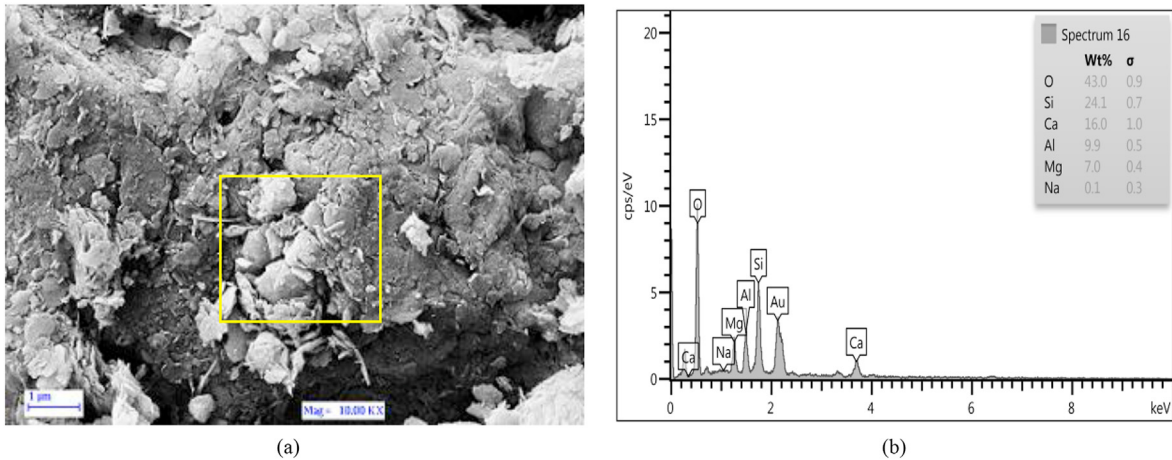
Fig. 2. (a) FESEM micrograph of the untreated soil, and (b) EDS analysis of the determined area.

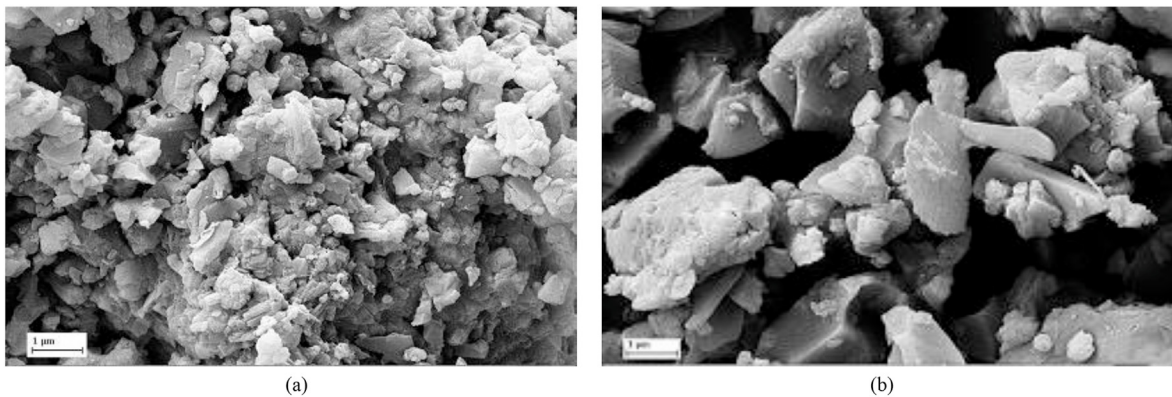(a)   (b)

Fig. 3. FESEM micrographs of (a) VA and (b) GGBS.

was also adopted in this study. However, futher research can be conducted to determine if the released heat in the hydration of NaOH can be utilized to increase the reaction rate in clayey soil stabilization. Since the quality of water has considerable impacts on the mechanical properties of cementitious materials, distilled water was used in all of the experiments (Sadeghi-Nik et al., 2011; Jahandari et al., 2017c, 2019, 2020, 2021a, b; Mohammadi et al., 2019, 2020; Afshar et al., 2020; Rasekh et al., 2020; Sadeghian et al., 2020, 2021; Mehdizadeh et al., 2021; Parsajoo et al., 2021).

3. Research program

3.1. Overview of experiments

Three sets of UCS tests were performed to investigate the influence of different factors on the strength and durability of alkali-activated VA/GGBS stabilized clayey soil. In Set 1, the effects of different ratios of VA/GGBS, different ratios of liquid to solid (L/S), two curing conditions (OC: cured in oven at 60 °C and AC: cured at ambient temperature), and different curing periods of 7 d, 28 d and 90 d were investigated. In Sets 2 and 3, the durability of some of the samples against W-D and F-T cycles was studied. It is worth mentioning that the L/S ratios were selected on a trial basis. Several samples were tested with different L/S ratios to find out the acceptable range. As shown in the XRF results, the soil is mainly composed of aluminosilicate, which has negative charges on its

surface with a high cation exchange capacity. Thus, the soil can absorb large amounts of positively charged cations (such as Na, K, Mg and Ca). Hence, when a lower amount of sodium hydroxide was used (L/S ratio <0.18), the strength was lower than that of the untreated soil because the precursor remained unreacted. On the other hand, the use of a large amount of sodium hydroxide is neither environmentally friendly nor cost-effective; thus, this research aimed to find an optimum L/S ratio by investigating the influence of different ratios on the mechanical properties. Summary of the test program and the utilized abbreviations for each sample is listed in Table 2. According to Table 2, for instance, M0A28 stands for the sample with the L/S ratio of 0.22, GGBS content of 0% of the binder mass, and cured at ambient temperature for 28 d.

Table 2
Program of experiments.

Set	VA/GGBS ratio	Liquid/solid	Curing condition	Curing time (d)	W-D cycle	F-T cycle
1	100/00, 85/15, 70/30, 55/45, 00/100	Low (L): 0.18, Medium (M): 0.22, High (H): 0.26	Ambient (AC), Oven (OC)	7, 28, 90		
2	100/00, 70/30	0.22	AC, OC	28		6, 12
3	100/00, 70/30	0.22	AC, OC	28	6, 12	

Table 3
Embodied carbon of materials.

Material	e_{CO_2} (kg/m³)	Reference
VA	0.041	Robayo-Salazar et al. (2018)
GGBS	0.019	Purnell (2013), Van den Heede and De Belie (2012)
Sodium hydroxide	1.915	Tan et al. (2020), Zannerni et al. (2020)
Water	0.0003	Long et al. (2015)

3.2. Sample preparation and curing

In this research, the clayey soil was first dried in oven at 105 °C for 2 d and then passed through a sieve #10 (2 mm) prior to use in the experiments. The total binder (VA+GGBS) content was fixed at 20% of the soil mass, and the VA was replaced by GGBS at 15% intervals (i.e. 0%, 15%, 30% and 45% of VA mass). To prepare the specimens, the VA and GGBS were first well blended using an automatic stainless steel mixer (Hobart N50-619 L 5 quart planetary mixer) for about 3 min until a homogeneous blend was achieved. Then, the activator in liquid form was added to the mixture and mixing process was resumed for 5 min. After that, the obtained slurry was well blended with the clayey soil for 5 min. The mixture was subsequently transferred to standard cylindrical moulds with a diameter of 50 mm and a height of 100 mm, and compacted in 3 layers via a steel rod with a diameter of 49 mm to eliminate air pockets. The samples were prepared with a compaction energy level by which they could reach their maximum dry density. Then, the prepared samples were demolded, placed in plastic bags, and cured in two conditions of ambient curing (AC) and oven curing (OC) for 7 d, 28 d and 90 d. Curing at 60 °C was followed to simulate the natural whether condition in some warm regions such as Kerman and Khoozestan Provinces located in Iran with the highest recorded temperature of 65 °C in summers (Saberian et al., 2017b). It is worth to mentioning that to avoid significant moisture loss during the curing process, the samples were properly sealed by plastic sheets. However, it would be difficult to avoid moisture loss in a practical application; hence, further research should be conducted to study the impact of moisture loss during curing on the mechanical properties. AC was performed in an AC chamber with a relative humidity of 80% ± 2% and a temperature of (25 ± 2) °C. For each test, at least three specimens were prepared and tested, and the average of which was reported as the representative value. The error bars representing the standard deviation are illustrated in the figures. Sample preparation for F-T cycles was in accordance with ASTM D560-16 (2016). In this regard, samples M0A28, M0O28, M30A28 and M30O28 were frozen at −23 °C for 24 h and were subsequently placed in a moist chamber with a relative humidity of 98% at ambient temperature for 23 h to become thawed. The W-D cycles were carried out based on ASTM D559-15 (2015). Hence, the abovementioned samples were submerged in water for 5 h and were then dried in an oven at (71 ± 3) °C for 42 h. The samples were exposed to 6 and 12 cycles of W-D and F-T.

3.3. Unconfined compression test

Unconfined compression tests were performed using a universal testing machine according to ASTM D2166-16 (2016) with a maximum capacity of 50 kN and loading rate of 1 mm/min. The diameters of all of the samples were measured by a digital calliper to modify the obtained UCS if needed.

3.4. Microstructural analysis

The VA and GGBS as well as the alkali-activated VA/GGBS stabilized soil samples were examined by XRD using an X'Pert Pro
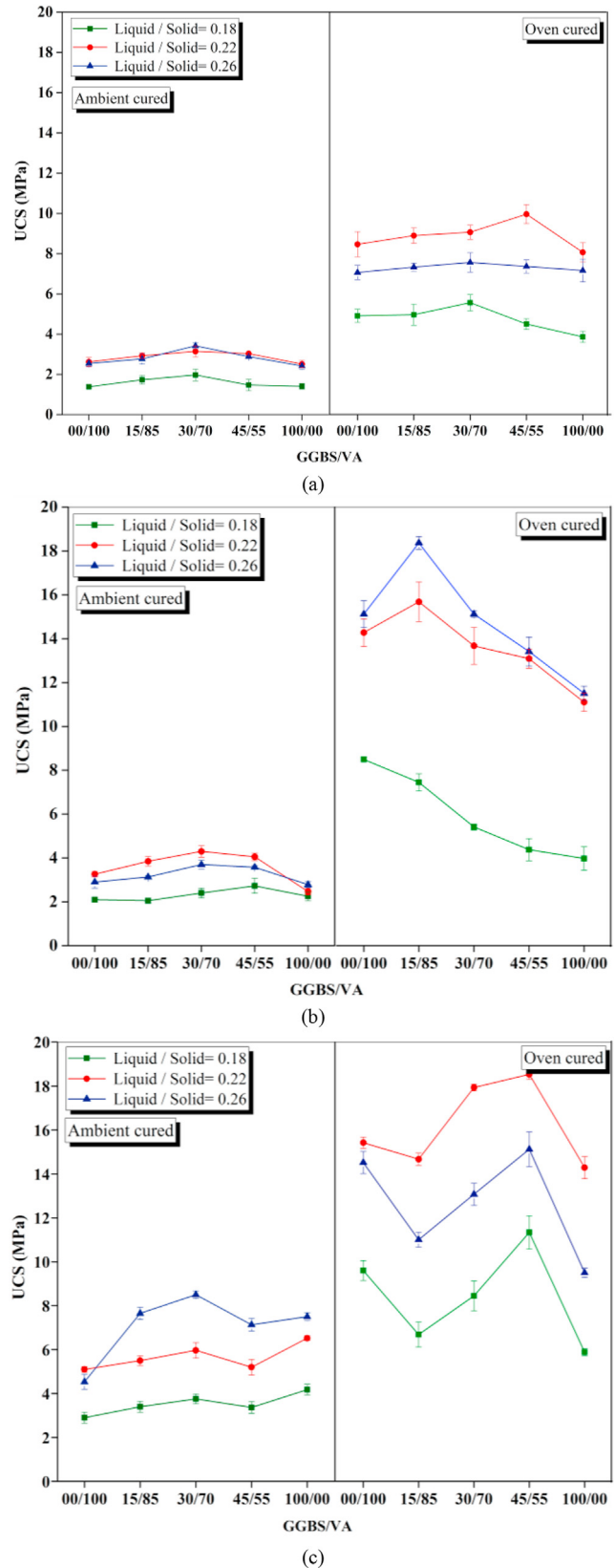

Fig. 4. The UCS values of (a) 7-d, (b) 28-d and (c) 90-d cured samples with different VA/GGBS and L/S ratios in the curing conditions of AC and OC.

devise of Panalytical Company with anode material of Cu, a step size of 0.026 and a 2θ range of 2°–80° operated at 40 kV and 40 mA.

Also, the powdered samples were pressed into KBr pellets to be prepared for FTIR analysis using an FTIR spectrometer device of PerkinElmer Company. FESEM and EDS via a ZEISS spectroscopy devise were used to study the microstructural properties of the powdered GGBS and VA as well as some of the stabilized clayey soil samples.

3.5. Sustainability analysis

The carbon footprint of stabilized samples with multiple mix designs were calculated according to Eq. (1) and Table 3 (Ma et al., 2020). The embodied carbon of each sample included extraction, processing, production and transportation of the binders and activator (Shi et al., 2019). However, since one of the primary aims of this study was to investigate the feasibility of gaining desirable strength and durability properties at ambient temperature, the embodied carbon was only calculated for the ambient-cured samples. It is clear that the same values could be adopted for the oven-cured samples provided that the warm natural temperature in the field is simulated in the oven, as assumed in this study. Otherwise, these values are not applicable for the oven-cured samples since a relatively huge amount of energy was consumed by the oven to cure these samples.

$$CI = \frac{e_{CO_2}}{UCS_{28\ d}} \tag{1}$$

where *CI* is the carbon index, e_{CO_2} is the carbon embodied (kg/m^3), and $UCS_{28\ d}$ is the compressive strength of each sample after being cured for 28 d.

4. Results and discussion

4.1. Unconfined compression test results

The impacts of various parameters such as L/S ratio, VA/GGBS ratio, curing periods, AC, OC, W-D cycles, and F-T cycles were investigated, and the results are discussed in the following sections. The results demonstrates that UCS values of the stabilized samples were enhanced compared with the untreated samples with a UCS value of 0.7 MPa; however, some of the stabilized samples did not meet the minimum strength of 2.068 MPa required by PCA (1992) for cement-stabilized base and subbase, which will be further discussed in the following.

4.1.1. Impact of L/S ratios

Fig. 4 demonstrates the UCS values of 7-d, 28-d and 90-d cured samples at curing conditions of AC and OC with different VA/GGBS and L/S ratios. As observed, low UCS values were obtained when the L/S ratio was 0.18. By increasing this ratio from 0.18 to 0.22, the UCS values of all samples increased; however, further increasing this ratio from 0.22 to 0.26 brought about different impacts at different curing times and conditions.

At lower L/S ratios, for example, L0A7, L30A7 and L100A7, samples had the UCS values of 1.38 MPa, 1.97 MPa and 1.41 MPa, respectively. These values are comparatively lower than their peer samples with the L/S ratio of 0.22 which respectively had the UCS values of 2.62 MPa, 3.14 MPa and 2.51 MPa. The lower strength values at L/S ratio of 0.18 could be attributed to the surplus of solid content which may have slowed down the geopolymerization reactions and hindered the extent of formed cementitious substances (Heah et al., 2012). This statement is later supported by FESEM/EDS analysis in Section 4.2.3. Provis et al. (2009) reported that geopolymers with very low L/S ratios mostly do not obtain high strength due to poor extent of gel formation. Moreover, in

geopolymer chemistry, the negative charges of final products reach equilibrium through the bonding of metal cations in polymeric network (Davidovits, 1994; Provis and Bernal, 2014). In other words, each Al atom needs one Na atom to be balanced (Zhang et al., 2010); hence, inadequate amounts of alkaline solution may have resulted in the incomplete dissolution of the precursors and adversely affected the degree of geopolymerization. Rise of the L/S ratio from 0.18 to 0.22 brought about higher UCS values in all of the samples; however, as it is indicated in Fig. 4a and b, further increasing the L/S ratio from 0.22 to 0.26 did not lead to strength development for 7-d and 28-d cured samples in AC condition, which could be due to the large volume of fluid in the medium that might have impeded the intermolecular contact between the binder and the activator (Topccedil and Uygunoğlu, 2010). Additionally, water has a significant impact on the performance of geopolymer by providing an environment for geopolymerization reactions. During the geopolymerization process, the dissolution of aluminosilicate constituents via alkaline hydrolysis consumes a considerable amount of water present in the system. Hence, with low amounts of water, the dissolution of aluminosilicate components could not be fully accomplished to form adequate cementitious materials which resulted in lower UCS values in samples with L/S ratio of 0.18. However, with the progress of geopolymerization reactions, a certain amount of water would be released through the condensation and polymerization of polymer monomers which would result in the formation of small holes in the path where the water flows leading to strength reduction. This is later confirmed by the microstructural observations in Section 4.2.3. Although the reduction in strength by increasing L/S ratio from 0.22 to 0.26 is obvious in the samples cured for 28 d in AC condition, the 7-d cured samples did not experience this reduction. This could be due to the short curing time of the samples with a high L/S ratio, which caused the mobility of ions to be lowered because of the electrostatic shielding. As a result, limited leaching of silica and alumina led to strength reduction (Zhao et al., 2020).

As indicated in Fig. 4, for the samples cured in OC condition, similar trends in the compressive strength were obtained by increasing the L/S ratio from 0.18 to 0.22, further increasing this ratio from 0.22 to 0.26 led to strength decline for 7-d and 90-d cured samples, while 28-d cured samples achieved higher strengths. To illustrate, at L/S ratio of 0.18, samples L30O7, L30O28 and L30O90 had the strength values of 5.6 MPa, 5.43 MPa and 8.45 MPa, respectively. By increasing the L/S ratio to 0.22, these values increased to 9.1 MPa, 13.46 MPa and 17.92 MPa, respectively. But, further increasing this ratio decreased the strength values of samples H30O7 and H30O90 to 7.6 MPa and 13.06 MPa, respectively, whereas in the case of H30O28, the strength increased to 15.1 MPa. The probable reasons for strength decline at higher L/S ratios are discussed above. In addition to the aforementioned explanations, destruction of the soil structure due to the formation of metallic hydroxides by reactions between the excess OH^- (released from NaOH) with soil cations (Bilondi et al., 2018) may account for the strength decline. In spite of all aforementioned reasons for strength decrease at high L/S ratio, Fig. 4b and c indicates that 28-d OC cured samples oven and 90-d AC cured samples did not experience strength reduction, which is related to the positive effect of curing time and curing condition. In other words, heat curing (in 28-d cured OC samples) and longer duration of curing (in 28-d cured AC samples) alleviated the negative effect of electrostatic shielding and prevented the samples from strength reduction.

Generally, considering that the 28-d UCS is often used as a benchmark in the filed implementation designs, the L/S ratio of 0.22 can be an appropriate ratio to be used in the areas with the average temperatures of around 25 °C. However, for the warm districts with the temperatures around 50 °C, the L/S ratio of 0.26

results in higher UCS values. Nevertheless, the L/S ratio of 0.22 could also be used in such warm regions because the UCS values of the samples prepared with this ratio also met the minimum strength of 2.068 MPa required by PCA (1992) for cement-stabilized base and subbase.

4.1.2. Effect of different VA/GGBS ratios

The results of previous studies showed that in most samples, replacing VA with GGBS up to an optimum amount led to strength improvement (Ismail et al., 2013; Parthiban et al., 2013). The combination of VA with GGBS provided sufficient amounts of silicon and calcium for geopolymerization reactions (Xu and Van Deventer, 2003) through which the calcium, aluminium and amorphous silicon were dissolved by the sodium present in the solution and subsequently formed monomers. The polycondensation of these monomers led to the formation of a strong geopolymeric network developed throughout the soil structure leading to soil stabilization (Hardjito and Rangan, 2005; Heah et al., 2012; Gao et al., 2013; Pourakbar et al., 2016).

Fig. 4a indicates that replacing VA with GGBS up to 30% in all samples cured in ambient condition led to strength enhancement. Since VA is a material with crystalline phase, it requires higher temperatures of about 50 °C–100 °C to become activated (Takeda et al., 2014; Djobo et al., 2017); while GGBS is a material with amorphous phase and its activation at ambient temperatures is more accessible leading to development of more C–S–H gel (Toghroli et al., 2020). Therefore, partial replacing of VA with GGBS brought about higher UCS values at ambient temperature. Additionally, as reported in previous studies, the more the calcium is present in the medium, the faster the pozzolanic reactions occur (Lin et al., 2007). Moreover, the amount of calcium can affect both the kinetics of the pozzolanic reactions and the amount of hydrated phases. Increasing the amount of calcium can lead to the formation of more calcium silicate or calcium aluminate hydrated phases during the process of polymerization (Lin et al., 2007). Furthermore, increasing the calcium concentration gradient can increase the rate of pozzolanic reactions. However, pozzolanic reactions can be divided into several stages, each of which can be controlled by the rate of the reactions, the diffusion of the reactants into the porous layer of the hydration products, or the diffusion of the reactants into the dense layer of the hydration (Shi and Day, 2000).

Moreover, since the reaction between GGBS and the alkaline solution is exothermic, the produced heat might have contributed in better reactions (Phoo-ngernkham et al., 2015).

One of the questions that arises is how calcium present in GGBS contributes to strength development. Although the presence of calcium component is not necessary in geopolymerization, calcium may affect the composition of the final product. The calcium components of the binders are dissolved in a high-alkaline medium to become free Ca^{2+} cations. Meanwhile, the aluminosilicates are dissolved by the activator to become Al and Si monomers. Free Ca^{2+} cations prefer to neutralize the negative charges resulting from the polymerization of Si and Al monomers prior to Na^+ (Fillenwarth and Sastry, 2015; Rashidian-Dezfouli et al., 2018). In other words, a definite amount of Ca^{2+} contributes to geopolymerization, as Ca^{2+} is a structure changing ion, increasing its content in the medium changes the gel product from N-A-S-H to (N,C)-A-S-H and further to C-(A)-S-H gel which will be clearly discussed in the FESEM/EDS analysis section (Yip et al., 2008). The coexistence of N-A-S-H gel and C-(A)-S-H gels filled the holes in the 3D geopolymer network, resulting in a denser and stronger geopolymer matrix (Phoo-ngernkham et al., 2015). Nevertheless, as demonstrated in Fig. 4b (the samples cured in AC condition) and Fig. 4a (the samples cured in both AC and OC conditions), further increasing the amounts of GGBS led to strength decrease which is attributed to the

occurrence of cracks as confirmed by FESEM micrographs. It has also been reported in the previous studies that the risk of cracking increases by using higher amounts of GGBS due to the high shrinkage of AAM (Ouyang et al., 2020). Although increasing the GGBS content from 30% to 45% and 45%–100% resulted in lower strength values for samples cured for 7 d and 28 d, the samples cured for 90 d experienced strength enhancement. This is due to the slower rate of pozzolanic reactions at ambient temperature; hence, longer curing periods led to more strength development.

As can be observed in Fig. 4a, increasing the GGBS content did not significantly affect the UCS values of 7-d cured samples in OC condition. This is due to the quicker precipitation and faster geopolymerization occurring on the surface of the undissolved particles owing to the accelerating impact of OC condition in a short curing period, all of which resulted in moisture loss and generated a poor geopolymeric network (Yaghoubi et al., 2019).

The results outlined in Fig. 4b demonstrate that for 28-d cured samples in OC condition, at L/S ratio of 0.18, the UCS values decreased with increasing GGBS content, while for the samples with L/S ratios of 0.22 and 0.26, increasing the GGBS content to 15% led to strength development and further increasing the GGBS content resulted in strength reduction. One explanation for strength reduction at L/S ratio of 0.18 could be lower amounts of water in the samples. In fact, heat curing leads to the diffusion of the moisture to the surface of the samples resulting in the dehydration of the mixture. From another point of view, GGBS went through both hydration and geopolymerization, while at L/S ratio of 0.18, GGBS was not provided with its required water for the reactions; hence, particles might have remained unreacted resulting in strength reduction. However, at L/S ratios of 0.22 and 0.26, not only more amount of alkali solution was available to react with GGBS and VA, but also the aqueous solution with stronger ionic strength facilitated the dissolution of glass particles resulting in strength increment up to 15% of GGBS incorporation (Xiao et al., 2020). However, by increasing calcium concentration, the formation of N-A-S-H and C-(A)-S-H gels could compete against each other for available space to grow; thus, instead of having one phase in filling out cavities, the final binder can be disordered with two phases having similar size leading to produce more holes and strength reduction (Yip et al., 2006).

Fig. 4c shows that at all of the L/S ratios of 0.18, 0.22 and 0.26, increasing the GGBS content up to 15% led to strength decrease in 90-d cured samples in OC condition. Further adding GGBS up to 45% resulted in strength development, while by reaching the GGBS content to 100%, samples experienced a reduction in their strength. When the amount of calcium in the medium is low, C–S–H gel formation is not possible; thus, the particles might have remained unreacted which account for the lower UCS values at 15% of GGBS (Yip et al., 2006). However, by introducing more GGBS, the coexistence of sufficient amounts of it with VA led to formation of a considerable amount of tetra coordinated Al charge which was balanced by Na, and formed gels in the hydrated Na_2O–CaO–Al_2O_3–SiO_2 system. Moreover, the dissolution of GGBS and VA through alkali activation can generate a higher degree of cross-linking in the matrix including both C–(A)–S–H and N–A–S–H gels (Ismail et al., 2014). However, as it is indicated in FESEM micrographs, when GGBS content was more than a certain amount, the geopolymeric gels developed progressively, and instead of creating a uniform network throughout the soil, the generated gels flocculated crystal particles which had some bonds with each other. As these crystals became larger with time, they commenced imposing forces on each other that resulted in some nonuniformity within the geopolymeric network and slight bond breakages, leading to a decrease in the strength values. This phenomenon usually occurs in an alkaline medium where water and

amorphous silica exist due to the alkali silica reactions in the mixtures (Pacheco-Torgal et al., 2012; Kupwade-Patil and Allouche, 2013). The hydroxyl ions attack the siloxane bonds and give rise to the formation of expansive gels that results in internal pressure in the microscale. The presence of GGBS, rich in calcium, intensified this phenomenon (Pacheco-Torgal et al., 2012; Kupwade-Patil and Allouche, 2013).

Again, considering that the 28-d UCS is often used as a benchmark in the filed implementation designs and provided that the L/S ratio suggested by the authors in the previous section is employed, VA/GGBS ratio of 70/30 can be an appropriate ratio to be used in the areas with the average temperatures of around 25 °C. However, for the warm districts with the temperatures around 50 °C, VA/GGBS ratio of 85/15 exhibits better mechanical properties.

4.1.3. Effects of curing conditions

Curing times and temperatures also have significant effects on the compressive strength of alkali-activated VA/GGBS. The samples cured at OC condition exhibited superb strengths which are tied to the effects of water and temperature on the geopolymerization.

The structural water, which is vital for geopolymerization, provides an environment for dissolution and hydrolysis of aluminosilicate materials and supplies a medium for ions transfer. This type of water is not evaporated at low temperatures (Kuenzel et al., 2012; Ranjbar et al., 2014). However, there is another type of water, called residual water, which is not desirable for the strength improvement as it decreases the matrix alkalinity through diluting the medium, and slows down the rate of geopolymerization reactions at hydrolysis and dissolution stages (Xu and Van Deventer, 2003; Pourakbar et al., 2016). The residual water is exclusively utilized to provide adequate workability (Ranjbar et al., 2017). By curing in oven, the alkalinity of the matrix increases gradually due to the evaporation of free water, while at ambient condition, high activator content retards the strength development of samples. In other words, when curing is performed at ambient temperature, usually longer times are required for the aluminosilicate to become dissolved sufficiently and accomplish the condensation process to gain desirable compressive strength. Therefore, by extending the curing period for the samples cured at AC condition, the UCS values increased remarkably from 7 d to 90 d. However, at OC condition for the samples with L/S ratio of 0.26, increasing the curing time from 28 d to 90 d led to strength reduction which could be due to the contraction of reaction products owing to excess shrinkage leading to development of shrinkage cracks in the specimens.

Additionally, it can be observed that the difference between the UCS values of 7-d cured samples and 28-d cured samples at AC condition was decreased by increasing the GGBS content from 0% to 45%. This can be attributed to the presence of more calcium, resulting in the acceleration of reactions kinetics by providing additional nucleation sites for the precipitation (Van Deventer et al., 2007). However, as previously explained, in OC condition, the UCS values of 7-d cured samples are significantly lower than those of 28-d cured samples.

Similar to the findings of this research, a previous study on geopolymer-stabilized soil samples cured in oven demonstrated a 200% enhancement in UCS values compared to the corresponding cement-stabilized samples. However, cement-stabilized soil had a superb performance at ambient temperature and exhibited 33% higher strength compared to the geopolymer-stabilized soil (Ghadir and Ranjbar, 2018).

4.1.4. Durability against W-D cycles

Fig. 5 demonstrates the performance of samples M0A28, M0O28, M30A28 and M30O28 against W-D cycles. The results showed that after 6 W-D cycles, samples M0A28, M0O28 and
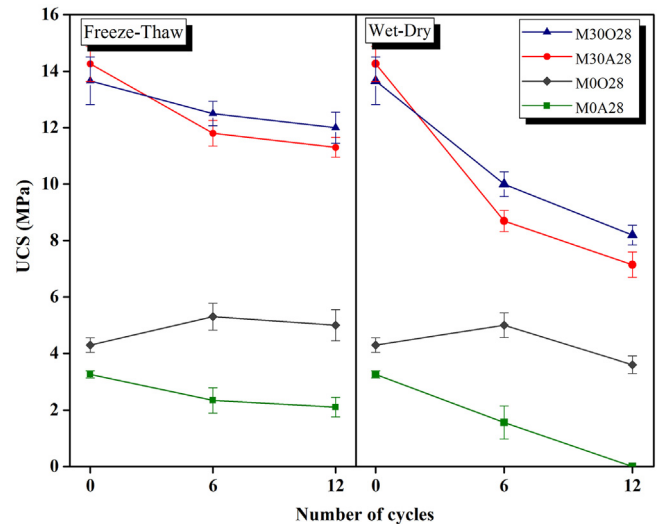

Fig. 5. UCS values of the 28-d cured samples after exposure to W-D and F-T cycles.

M30O28 experienced 52%, 39% and 27% reduction in their strength values, respectively, while the strength of sample M30O28 increased by 17%. However, a general strength reduction was observed for all of the samples exposed to more than 6 cycles (i.e. 12 cycles of W-D). The strength reduction from 6 to 12 cycles was gentler compared with 0–6 cycles. Moreover, all 3 M0R28 samples failed to bear 12 cycles and collapsed at the 10th cycles.

The results show that introducing GGBS into the mixture as well as curing in oven improved the resistance of samples against W-D cycles. The soaked condition demonstrates the most severe possible scenario of utter saturation for the stabilized soil in the project sites. Since the effective stress generated by capillary phenomenon accounts for the instant un-soaked UCS (Raymon, 1961), the inundation of the accessible void spaces by water brings about a dramatic decline in surface tension forces leading to strength reduction. However, introducing GGBS as well as curing in OC condition resulted in better performance against W-D cycles due to better cementation of particles by promoted pozzolanic reactions. Surprisingly, the samples with the VA/GGBS ratio of 70/30 that were cured at ambient temperature experienced strength development during first 6 cycles which can be explained as follows. At this stage, the principal contributor to the strength development is C–S–H (Du et al., 2016). In the soaking process, the leaching of calcium from the binders can participate in the development of the cementitious products (Du et al., 2014). As long as the remaining calcium is accessible, the pozzolanic reactions will last resulting in the formation of calcium hydrates on account of the presence of Ca^{2+}, OH^-, SiO_4 and AlO_6 ions. Additionally, drying at 70 °C in the process of W-D cycles, apparently contributed in the development of cementitious products (C-A-S-H) (Brue et al., 2012; Jiang and Yuan, 2013), i.e. an increased temperature leads to a quicker diffusion of moisture and therefore rapid chemical reaction (Drouet et al., 2015; Wang et al., 2016). Previous studies which investigated the performance of fly ash stabilized with lime and gypsum against W-D cycles also demonstrated the strength increase owing to the development of cementitious products during W-D cycles (Drouet et al., 2015). The strength reduction for the other samples in the first 6 cycles and for all of the samples from 6th to 12th cycle could be attributed to the crack propagation on account of the desiccation kinetics leading to the moisture loss (Aldaood et al., 2014), followed by the inundation of pore spaces and cracks with water during the wetting process. Additionally, the dissolution of geopolymer gels due to soaking might be another reason for the strength reduction.

The results of a previous research (Ghadir et al., 2021b) conducted on a sandy soil stabilized by VA-based geopolymer demonstrated that in both curing conditions of OC and AC, cement-stabilized soil had better resistance to W-D cycles compared with geopolymer-stabilized samples. However, the findings of the current research showed that by the introduction of GGBS and adoption a proper VA/GGBS ratio, the samples could favourably resist against all 12 W-D cycles in both curing conditions and met the minimum requirement of 2.068 MPa for cement-stabilized base and subbase.

4.1.5. Durability against F-T cycles

Fig. 5 demonstrates the performance of samples M0A28, M0O28, M30A28 and M30O28 against F-T cycles. The results demonstrated that after 6 F-T cycles, samples M0A28, M0O28 and M30O28 experienced 28%, 17% and 9% reduction in their strengths, respectively, while sample M30O28 experienced a 23% strength increment. The strength remained approximately constant for all of the samples by being exposed to more 6 cycles (i.e. 12 cycles of F-T). The reasons mentioned in the previous section for strength development of M30A28 is also convincing for the performance of this sample during the initial 6 cycles of freezing and thawing. To shade light on the positive effect of GGBS, the production of C—S—H gel should be mentioned through which it bridged the unreacted particles and different hydrated phases; hence, it filled out the voids and pores resulting in less available cavities for water penetration and ice crystal formation. The strength reduction during F-T cycles was due to the volume increase of pores because of the expansion of water. As the activator content was higher than the optimum moisture content of the soil, the occurred expansion fully filled out the pores volumes and even further increased the pore volumes leading to detrimental impacts in the integrity of the matrix.

The results of a previous research (Ghadir et al., 2021b) demonstrated that after being exposed to 12 F-T cycles, geopolymer-stabilized samples cured in oven had higher strength values than cement-stabilized samples, whereas at ambient temperature, cement-stabilized samples exhibited better performance. However, the findings of the current research showed that by the introduction of GGBS and adoption of 70/30 as VA/GGBS ratio, the samples could successfully resist all 12 F-T cycles in both curing
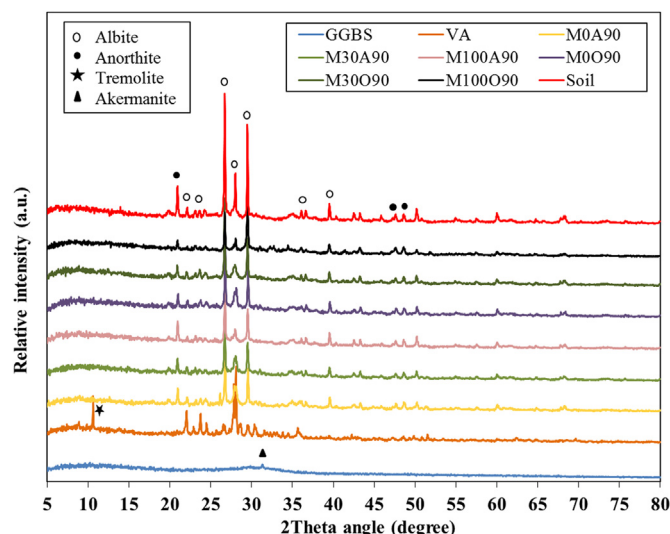

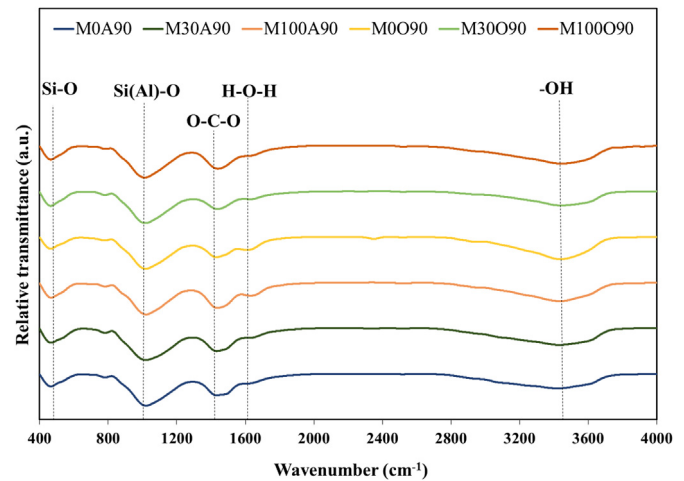**Fig. 6.** XRD patterns of the binders, untreated soil and stabilized samples.

Fig. 7. FTIR spectra of the stabilized samples.

conditions and met the minimum requirement of 2.068 MPa specified by PCA (1992).

4.2. Microstructural analysis

4.2.1. XRD analysis

Fig. 6 shows the XRD patterns of the untreated soil, VA, GGBS, M0A90, M0O90, M30A90, M30O90, M100A90 and M100O90. It is an obvious issue that the reactivity of aluminosilicate substances is directly tied to the level of amorphization. As indicated in Fig. 6, the XRD pattern of GGBS exhibited an evident broad hump which is distributed all along the spectrum without any sharp peaks, confirming the presence of ample amorphous phase. The only crystalline phase which was observed in GGBS pattern was Akermanite ($Ca_4Mg_{1.42}Al_{1.02}Si_{3.48}O_{14}$) which was detected at 2θ of $31.5°$. As expected, VA exhibited several crystalline phases including albite ($AlNaO_8Si$), sodium anorthite ($Al_{1.66}Ca_{0.68}Na_{0.3}O_8Si_{2.34}$), and tremolite ($Ca_2Mg_5Si_8O_{22}(OH)_2$). After the alkaline activation reactions, the intensity of the crystalline phase peaks as well as the amount of amorphous phase changed. To calculate the amount of amorphous phase, a quantitative analysis was carried out on the XRD data using Origin Pro software in the following procedure: (1) determine the baseline; (2) calculate the percentage of crystalline phases by calculating the area under the peak diagrams; and (3) obtain the percentage of amorphous phase by subtracting the percentage of crystalline phases from 100%. It was found that the samples M0O90, M30O90, M100O90, M0A90, M30A90 and M100A90 have amorphous amounts of 64.08%, 66.83%, 62.46%, 60.27%, 61.92% and 59.27%, respectively. This indicates that the alkaline activation of VA and GGBS, in addition to the development of geopolymerization reactions of the amorphous phase of the materials, has also caused some changes in the intensity of the crystalline phase compounds of the material. Since the anorthite and albite phases do not inherently exhibit any binding or latent hydraulic characteristics, the strength of the geopolymer samples is attributable to the changes occurred in the amorphous phase of the starting materials. It seems that the change of curing conditions does not affect the type of crystalline phases of geopolymer samples except their intensity, confirming that the observed changes in UCS are due to the changes in the amorphous phase. From the results of the quantitative analysis of amorphous phase, it is found that the samples cured in dry condition had more amorphous phase (62%–66%) than the samples cured at ambient temperature (59%–62%). The XRD pattern of the sample M0A90 shows that the intensity of the albite

crystalline phase was reduced; in contrast, the intensity of the anorthite crystallite phase was increased. Also, the tremolite crystalline phase of VA is utterly destroyed due to the chemical activation and the formation of C–S–H gel. Moreover, the crystalline phases of the samples M30A90 and M100A90 were similar to each other and only their amorphous phase was increased, leading to strength development by GGBS increment. However, the sample M100O90 exhibited a less amorphous phase than the samples M0O90 and M30O90, which might be due to the different natures of the amorphous gels formed in their matrix. Generally, XRD patterns confirmed that introducing GGBS weakened the intensity of the crystalline phase peaks and increased the amount of amorphous phase. Similar results have been reported in previous studies as well (Lemougna et al., 2020).

4.2.2. FTIR results

The main bands observed in the infrared spectra of samples M0A90, M0O90, M30A90, M30O90, M100A90 and M100O90 are illustrated in Fig. 7. The absorption bands appeared in the wavenumber of 468–475 cm^{-1} and also the bands in the wavenumber of 1000 cm^{-1} are attributed to the flexural vibrations of Si–O bonds in the tetrahedral SiO_4, the symmetrical vibrations of Si–O–Si bonds and tensile vibrations of Si–O–Al bonds (Torres-Carrasco et al., 2015; Lemougna et al., 2016; Tchakouté et al., 2017; Zawrah et al., 2018). These adsorption bands are common in the FTIR spectra of aluminosilicate materials and are known as the primary feature of the molecular structure of geopolymers.
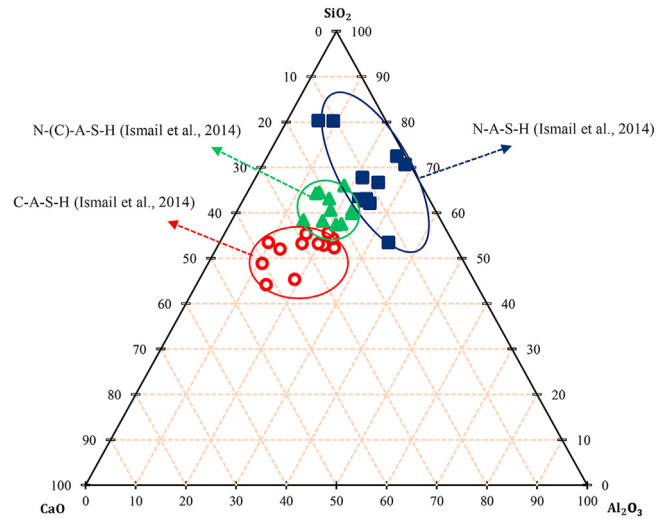
Fig. 9. Si_2O–CaO–Al_2O_3 ternary diagram of samples M0A90, M30A90 and M100A90.

These two adsorption bands are also sensitive to Si and Al contents. As Al–O bonds are weaker than Si–O bonds, the displacement of these two bands to lower wavelengths can be attributed to the replacement of tetrahedral structures of AlO_4 with SiO_4 due to the growth of geopolymerization reactions and the
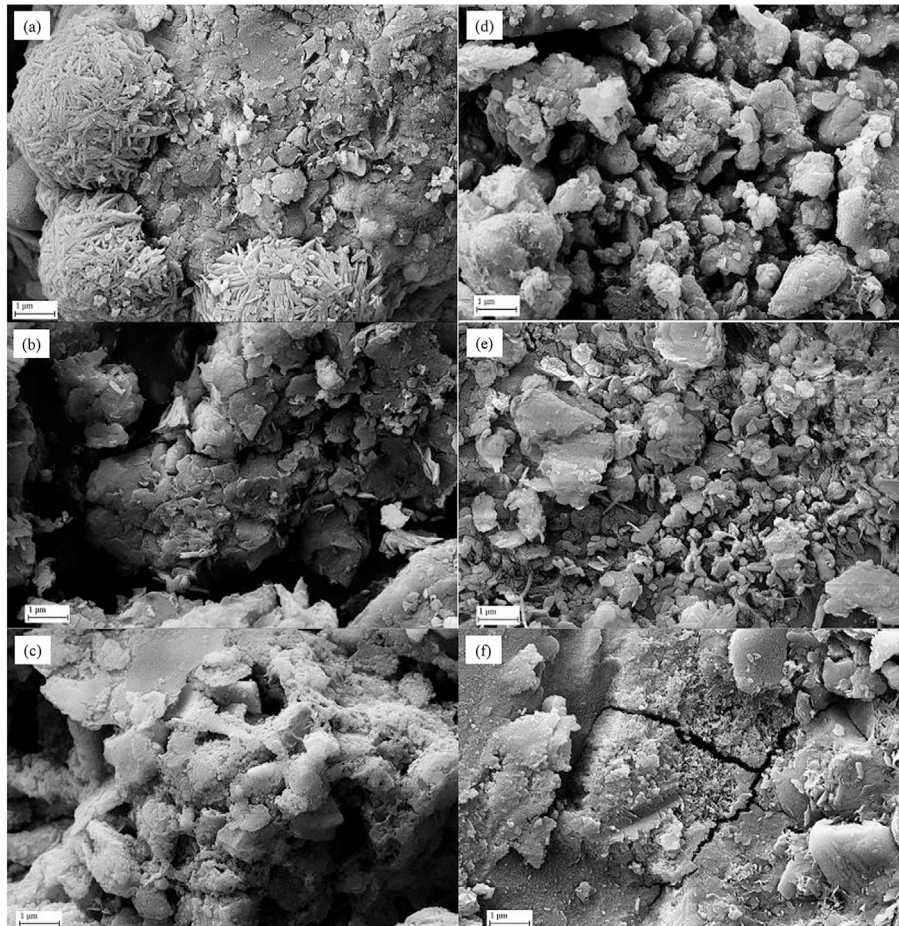
Fig. 8. FESEM micrographs of the stabilized samples (a) M0A90, (b) M30A90, (c) M100A90, (d) M0O90, (e) M30O60 and (f) M100O90.

development of the interconnected geopolymer network (Davidovits, 2008; Panagiotopoulou et al., 2015). The absorption bands in the wavelengths of 1643–1660 cm^{-1} are related to crystalline water and the absorption bands observed in the wavenumbers of 3435–3445 cm^{-1} correspond to the physical water (Lemougna et al., 2017b; Kaze et al., 2018). This water has either been superficially adsorbed on the material or trapped in the cavities of the geopolymer structure. The absorption bands appeared in the wavenumber from 1438 cm^{-1} to 1452 cm^{-1} represent the asymmetric tensile bonds of O–C–O, which are usually formed due to the carbonation of geopolymeric materials (Clayden et al., 1999; Criado et al., 2007).

4.2.3. FESEM, EDS and mapping analysis

Fig. 8 shows the FESEM micrographs of samples M0A90, M30A90, M100A90, M0O90, M30O90 and M100O90. Also, SiO$_2$–CaO–Al$_2$O$_3$ ternary diagram of samples M0A90, M30A90 and M100A90 is indicated in Fig. 9. The FESEM micrograph of sample M0A90 revealed that after alkaline activation of VA, a new morphology was formed in the matrix that bonded the soil particles to each other. As the amount of GGBS increased, the binder matrix became denser, as it is quite obvious in the microstructure of the sample M100A90, soil particles were connected to each other more integrally through N-A-S-H and (N, C)-A-S-H gels which was also observed in ternary diagram. By increasing the amount of GGBS in the binder composition, as seen in the FESEM micrograph of sample M30O90, the microstructure became denser and the formation of C-(A)-S-H and (N, C)-A-S-H gels was highly probable. As the amount of GGBS increased to 100% in the sample M100O90, structural cracks were seen in the matrix. These microcracks might be formed due to the formation of two or more kinds of gels in the microstructure. These gels are not integrated with each other and therefore cannot form a more compact microstructure. In addition, as the amount of GGBS increases, the amount of excess calcium in the reaction medium hinders the mobility of ions and polymer chains formation, resulting in the rapid precipitation of aluminosilicate gel. The precipitated gel consequently induces a microstructural stress in the geopolymeric network, leading to strength reduction (Qiu et al., 2019).

EDS results attained for multiple points (i.e. excluding the unreacted particles) of the various stabilized samples, including M0A90, M30A90 and M100A90, are indicated in Fig. 10. Silicon, calcium and aluminium contents of multiple points of the samples

are reported, renormalized on an oxide basis to 100% for being plotted on the ternary diagrams (i.e. disregarding the other existing elements). These plots vividly show the shifting in gel composition across different VA/GGBS ratios. The cluster of blue rectangular shapes corresponds to samples M0A90 whose detected binding phase is N-A-S-H, the famous geopolymer-type gel. The cluster of rectangular shapes refers to samples M30R90 whose detected binding phase is a type of gel with some contents of calcium that can be related to N–(C)–A–S–H gel. In other words, some of the Na$^+$ ions may have been replaced with Ca^{2+} ions resulting in the formation of a low-calcium gel. These findings are similar to the gel reported in a research for the specimen with combination of 75% fly ash with 25% GGBS (Ismail et al., 2014). The cluster of circles corresponds to multiple points of sample M100A90 whose observed binding phase is C-A-S-H resulting from the alkali activation of GGBS.

Among the stabilized soil samples, the sample M30O90 showed the highest compressive strength. Therefore, the elemental distribution mapping of this sample is shown in Fig. 10. A relatively uniform distribution of calcium, aluminium, sodium and silicon elements is observed, which is related to the proper formation of C-(A)-S-H and N-A-S-H gels in the geopolymer structure.

Fig. 11 depicts the FESEM micrographs of samples L30A90, M30A90, H30A90, L30O90, M30O90 and H30O90. Based on the results of unconfined compression tests, the compressive strength of the samples with VA/GGBS of 70/30 cured for 90 d in AC condition increased with increasing L/S ratio. As observed in the FESEM micrograph of the sample L30A90, the microstructure consisted of C–S–H and N-A-S-H gels. As mentioned earlier, the weaker strengths of samples with an L/S ratio of 0.18 can be related to the hindered geopolymerization reactions due to the high amount of unreacted precursor materials. This is supported by the FESEM/EDS analysis shown in Fig. 12. As can be seen, the chemical composition in the marked regions is close to that of the raw materials. Moreover, as argued in Section 4.1.1, the formation of small pores due to the water released during geopolymerization reactions is one of the important reasons responsible for the strength reduction of the samples. This is clearly observed in Fig. 13, in which small pores are shown by circles.

In the sample M30A90, the amount of N-A-S-H gel was increased which was due to the increment in the L/S ratio from 0.18 to 0.22. The sample H30A90, in which the L/S ratio was 0.26, most of
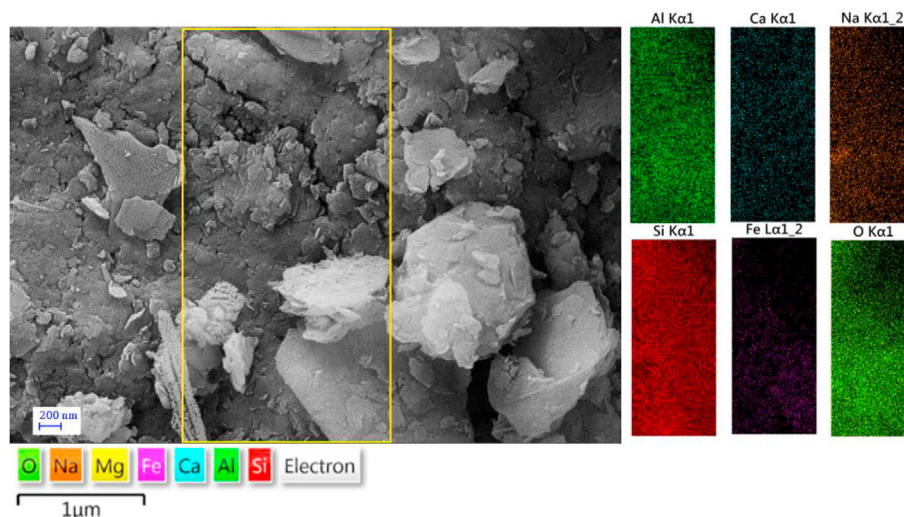

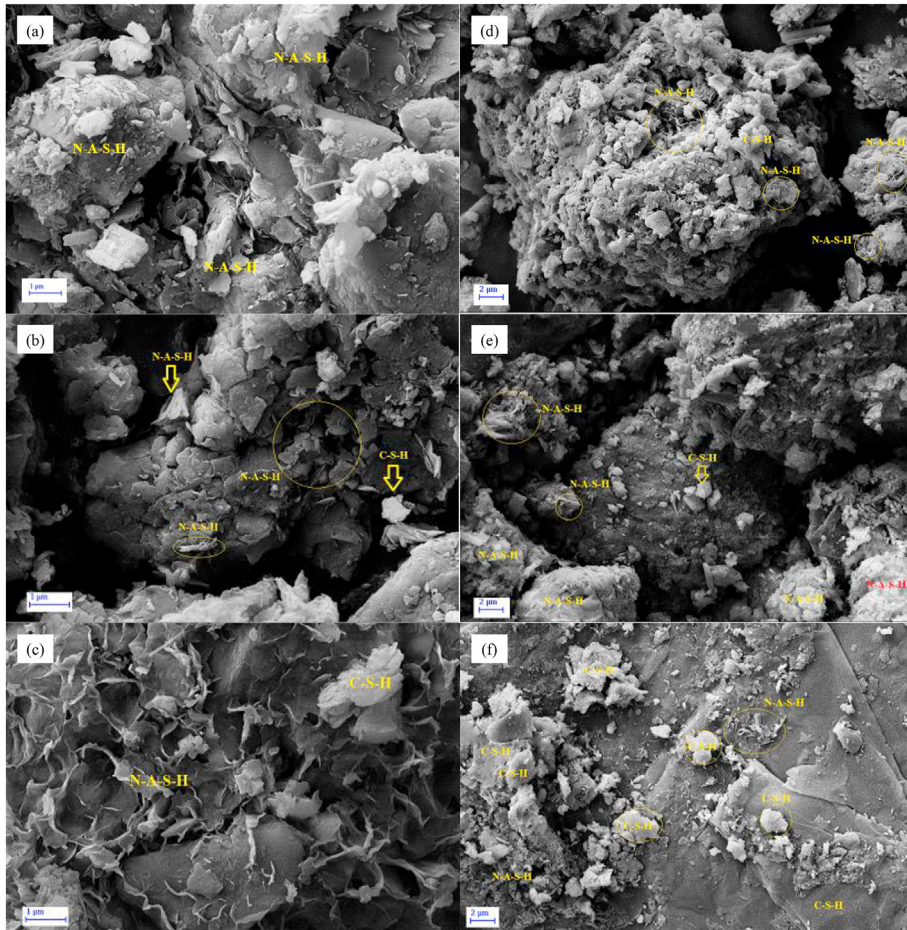**Fig. 10.** Elemental mapping of the microstructure of sample M30O90.

Fig. 11. FESEM micrographs of samples (a) L30A90, (b) M30A90, (c) H30A90, (d) L30O90, (e) M30O90 and (f) H30O90.
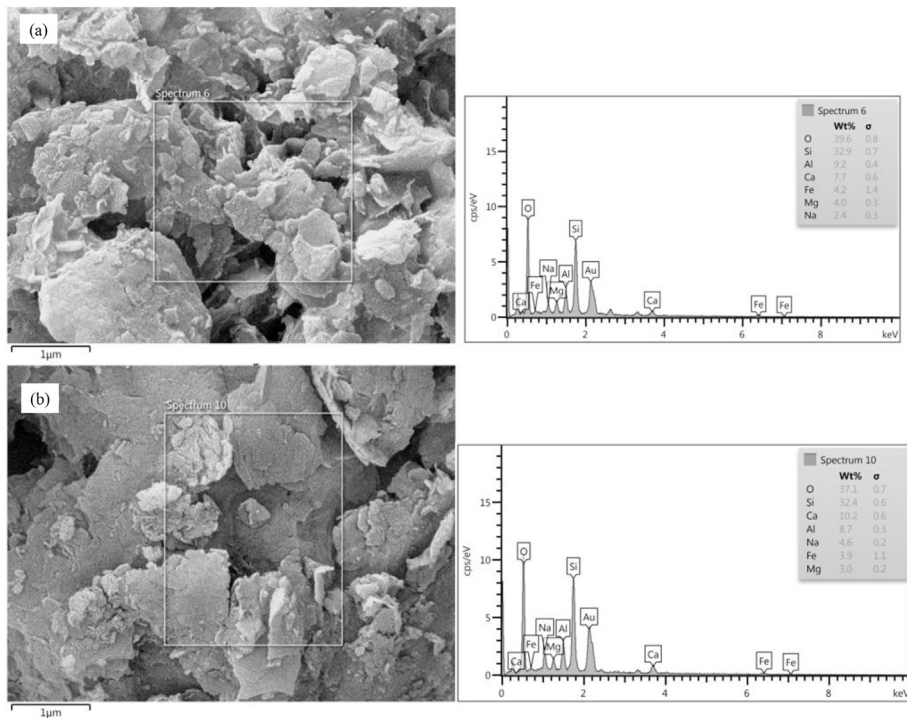

Fig. 12. FESEM/EDS analysis of samples (a) L30O7 and (b) L30A7 prepared with L/S ratio of 0.18.
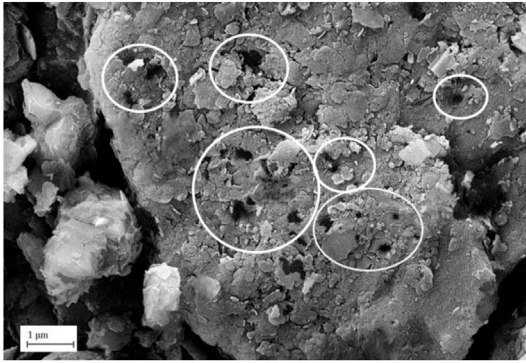
Fig. 13. FESEM micrograph of a 28-d cured geopolymer sample prepared with L/S ratio of 0.18.

formed binding phase is N-A-S-H gel, such morphology for N-A-S-H gel has already been reported in a previous research (Tambara Júnior et al., 2018). The obtained micrographs elucidate the compressive strength development of the mentioned samples. As previously discussed, in the case of samples cured in oven for 90 d with VA/GGBS of 70/30, increasing the L/S ratio from 0.18 to 0.22 led to strength increase, while increasing this ratio to 0.26 decreased the compressive strength. In FESEM micrograph of the sample L30O90, it can be seen that most of the binding phase formed are C–S–H and C-A-S-H gels and small traces of N-A-S-H gel are seen in the microstructure. In the sample M30O90, the dominant binding phase observed was N-A-S-H gel which was due to the increment of L/S ratio from 0.18 to 0.22. In the sample H30O90, in which the L/S ratio was 0.26, C–S–H gel became the dominant gel due to the degradation of the structure of N-A-S-H gel caused by the dissolution of its structural alumina in the severe alkaline environment leading to strength decline.

4.3. Carbon footprint evaluation

Embodied carbon and carbon index (CI) of the 28-d cured samples are demonstrated in Fig. 14. As observed, among the materials used for the sample preparation, NaOH is responsible for the highest CO_2 emission; however, the technology of producing NaOH is in progress. In 2013, the manufacture of more ecofriendly NaOH in Malaysia was reported, which can have a remarkable role in the geopolymer industry development. Moreover, replacing VA with GGBS resulted in lower carbon embodied and subsequently lower CI values which indicate the better sustainability of the samples containing more GGBS and less VA.

5. Conclusions

Lime and Portland cement are the most widely used binders in soil stabilization projects. However, due to the high carbon emission in cement production, research on soil stabilization by the use of more environmentally-friendly binders with lower carbon footprint has attracted much attention in recent years. This research investigated the potential of using alkali-activated GGBS and VA as green binders in soil stabilization projects, which has not been studied before. According to the results, the following main conclusions could be drawn:

(1) Increasing the L/S ratio had different results at different curing times and conditions, but generally it can be concluded that higher L/S ratios had detrimental impacts on the strengths of samples in OC condition, while at AC condition, higher L/S ratios led to the strength development particularly at longer durations of curing.

(2) Using a proper combination of VA with GGBS provided sufficient amounts of calcium, silicon and aluminium, leading to the formation of N-A-S-H and C-(A)-S-H gels. The coexistence of these gels filled the holes in the 3D material
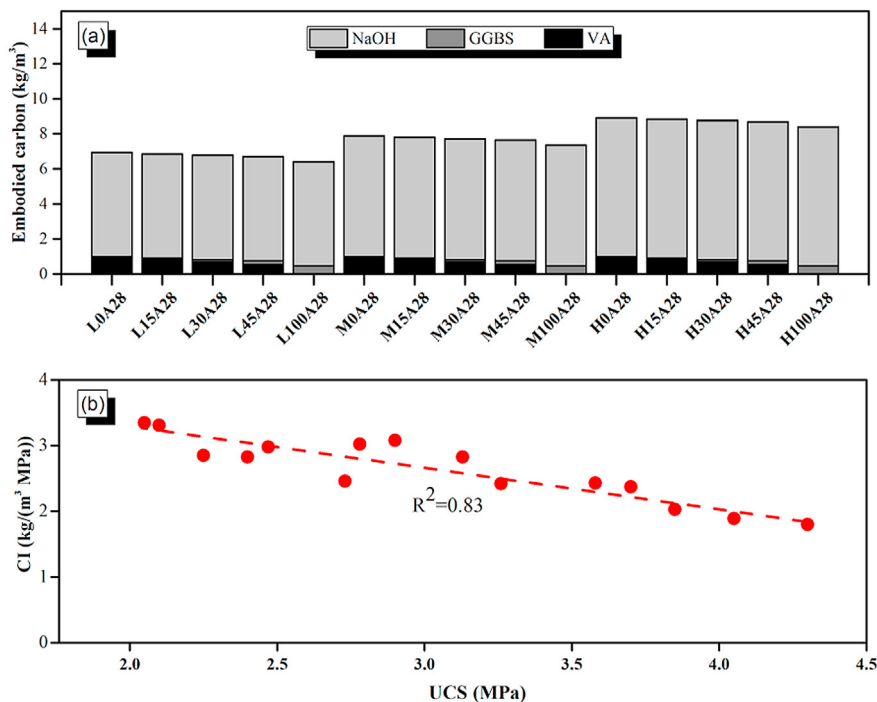

Fig. 14. Sustainability analysis of (a) embodied carbon and (b) CI for the 28-d cured sample.

network, resulting in a denser and stronger matrix and consequently higher strength values.

(3) VA requires higher temperatures to become activated, while GGBS has a desirable reactivity at ambient temperature, utilizing a mixture of these two materials enabled them to become applicable in wider ranges of temperatures including ambient temperature. The difference between the strength values of 7-d and 28-d cured samples at AC condition decreased by increasing the GGBS content from 0% to 45%, which implies the accelerated reactions kinetics as a result of providing additional nucleation sites for the precipitation.

(4) The ambient-cured samples with the GGBS content of zero did not meet the strength requirements after being exposed to W-D cycles. However, by the introduction of GGBS and taking advantage of a proper combination of VA AND GGBS, the samples cured in both conditions could favourably resist against all 12 W-D and F-T cycles and met the minimum strength of 2.068 MPa specified by PCA (1992) for cement-stabilized base and subbase.

(5) XRD patterns confirmed that introducing GGBS weakens the intensity of the crystalline phase peaks and increases the amount of amorphous phase. However, changing the curing condition apparently does not affect the crystalline parts of the geopolymer confirming that the observed changes in strength values are due to the changes in the amorphous phase.

(6) FESEM/EDS analysis confirmed the formation N-(C)-A-S-H gel in the presence of a proper combination of VA with GGBS, accounting for the strength development with the introduction of GGBS.

(7) Replacing VA with GGBS brought about lower carbon embodied and consequently lower carbon index (CI) values which indicates the better sustainability of the samples containing more GGBS and less VA.

Data availability statement

All data from experiments that support the findings of this study are available from the corresponding author upon request.

Declaration of competing interest

The authors declare that they have no known competing financial interests or personal relationships that could have appeared to influence the work reported in this paper.

Acknowledgments

References

Afshar, A., Jahandari, S., Rasekh, H., Shariati, M., Afshar, A., Shokrgozar, A., 2020. Corrosion resistance evaluation of rebars with various primers and coatings in concrete modified with different additives. Construct. Build. Mater. 262, 120034.

Aldaood, A., Bouasker, M., Al-Mukhtar, M., 2014. Impact of wetting—drying cycles on the microstructure and mechanical properties of lime-stabilized gypseous soils. Eng. Geol. 174, 11—21.

Andini, S., Cioffi, R., Colangelo, F., Grieco, T., Montagnaro, F., Santoro, L., 2008. Coal fly ash as raw material for the manufacture of geopolymer-based products. J. Waste Manag. 28 (2), 416—423.

ASTM 2487-11, 2011. Standard Practice for Classification of Soils for Engineering Purposes (Unified Soil Classification System). ASTM International, West Conshohocken, PA, USA.

ASTM D422-63, 2002. Standard Test Method for Particle-Analysis of Soils. ASTM International, West Conshohocken, PA, USA.

ASTM D423-66, 1972. Standard Method of Test for Liquid Limit of Soils. ASTM International, West Conshohocken, PA, USA.

ASTM D424-54, 1982. Standard Method of Test for Plastic Limit. ASTM International, West Conshohocken, PA, USA.

ASTM D559-15, 2015. Standard Test Methods for Wetting and Drying Compacted Soil-Cement Mixtures. ASTM International, West Conshohocken, PA, USA.

ASTM D560-16, 2016. Standard Test Methods for Freezing and Thawing Compacted Soil-Cement Mixtures. ASTM International, West Conshohocken, PA, USA.

ASTM D1557-09, 2009. Standard Test Methods for Laboratory Compaction Characteristics of Soil Using Modified Effort. ASTM International, West Conshohocken, PA, USA.

ASTM D2166-16, 2016. Standard Test Method for Unconfined Compressive Strength of Cohesive Soil. ASTM International, West Conshohocken, PA, USA.

ASTM D7928-17, 2017. Standard Test Method for Particle-Size Distribution (Gradation) of Fine-Grained Soils Using the Sedimentation (Hydrometer) Analysis. ASTM International, West Conshohocken, PA, USA.

Bahmani, M., Fatehi, H., Noorzad, A., Hamedi, J., 2019. Biological soil improvement using new environmental bacteria isolated from northern Iran. Environ. Geotechnol. https://doi.org/10.1680/jenge.18.00176z.

Bilondi, M.P., Toufigh, M.M., Toufigh, V., 2018. Experimental investigation of using a recycled glass powder-based geopolymer to improve the mechanical behavior of clay soils. Construct. Build. Mater. 170, 302—313.

Brue, F., Davy, C.A., Skoczylas, F., Burlion, N., Bourbon, X., 2012. Effect of temperature on the water retention properties of two high performance concretes. Cement Concr. Res. 42 (2), 384—396.

Buchwald, A., Kaps, C., Hohmann, M., 2003. Alkali-activated binders and pozzolan cement binders — complete binder reaction or two sides of the same story. In: Proceedings of the 11th International Congress on the Chemistry of Cement (ICCC), Durban, South Africa, pp. 238—246.

Bushlaibi, A.H., Alshamsi, A.M., 2002. Efficiency of curing on partially exposed high-strength concrete in hot climate. Cement Concr. Res. 32 (6), 949—953.

Chew, S., Kamruzzaman, A., Lee, F., 2004. Physicochemical and engineering behavior of cement treated clays. J. Geotech. Geoenviron. Eng. 130 (7), 696—706.

Clayden, N., Esposito, S., Aronne, A., Pernice, P., 1999. Solid state 27Al NMR and FTIR study of lanthanum aluminosilicate glasses. J. Non-Cryst. Solids 258 (1—3), 11—19.

Criado, M., Fernández-Jiménez, A., Palomo, A., 2007. Alkali activation of fly ash: effect of the SiO_2/Na_2O ratio: Part I: FTIR study. Microporous Mesoporous Mater. 106 (1—3), 180—191.

Cristelo, N., Glendinning, S., Teixeira Pinto, A., 2011. Deep soft soil improvement by alkaline activation. Proc. Inst. Civil Eng.-Ground Improv. 164 (2), 73—82.

Cristelo, N., Glendinning, S., Fernandes, L., Pinto, A.T., 2013a. Effects of alkaline-activated fly ash and Portland cement on soft soil stabilisation. Acta. Geotech. 8 (4), 395—405.

Cristelo, N., Soares, E., Rosa, I., Miranda, T., Oliveira, D.V., Silva, R.A., Chaves, A., 2013b. Rheological properties of alkaline activated fly ash used in jet grouting applications. Construct. Build. Mater. 48, 925—933.

Davidovits, J., 1991. Geopolymers — inorganic polymeric new materials. J. Therm. Anal. 37 (8), 633—656.

Davidovits, J., 1994. Properties of geopolymer cements. In: Proceeding of the 1st International Conference on Alkaline Cements and Concretes. Kiev State Technical University. Scientific Research Institute, Ukraine, pp. 131—149.

Davidovits, J., 2008. Geopolymer Chemistry and Applications, second ed. Institute Geopolymere, Saint-Quentin, France.

Djobo, J.N.Y., Elimbi, A., Tchakouté, H.K., Kumar, S., 2017. Volcanic ash-based geopolymer cements/concretes: the current state of the art and perspectives. Environ. Sci. Pollut. Res. Int. 24 (5), 4433—4446.

Dodson, V.H., 1990. Pozzolans and the pozzolanic reaction. In: Concrete Admixtures. Springer, 159-120.

Drouet, E., Poyet, S., Torrenti, J.-M., 2015. Temperature influence on water transport in hardened cement pastes. Cement Concr. Res. 76, 37—50.

Du, Y.-J., Wei, M.-L., Reddy, K.R., Liu, Z.-P., Jin, F., 2014. Effect of acid rain pH on leaching behavior of cement stabilized lead-contaminated soil. J. Hazard Mater. 271, 131—140.

Du, Y.-J., Bo, Y.-L., Jin, F., Liu, C.-Y., 2016. Durability of reactive magnesia-activated slag-stabilized low plasticity clay subjected to drying—wetting cycle. Eur. J. Environ. Civ. Eng. 20 (2), 215—230.

Du, Y.-J., Yu, B.-W., Liu, K., Jiang, N.-J., Liu, M.D., 2017. Physical, hydraulic, and mechanical properties of clayey soil stabilized by lightweight alkali-activated slag geopolymer. J. Mater. Civ. 29 (2), 04016217.

Farhangi, V., Karakouzian, M., Geertsema, M., 2020. Effect of micropiles on clean sand liquefaction risk based on CPT and SPT. Appl. Sci. 10, 3111.

Fillenwarth, B.A., Sastry, S.M., 2015. Development of a predictive optimization model for the compressive strength of sodium activated fly ash based geopolymer pastes. Fuel 147, 141—146.

Gao, K., Lin, K.-L., Wang, D., Hwang, C.-L., Tuan, B.L.A., Shiu, H.-S., Cheng, T.-W., 2013. Effect of nano-SiO_2 on the alkali-activated characteristics of metakaolin-based geopolymers. Construct. Build. Mater. 48, 441—447.

Ghadir, P., Ranjbar, N., 2018. Clayey soil stabilization using geopolymer and Portland cement. Construct. Build. Mater. 188, 361—371.

Ghadir, P., Zamanian, M., Mahbubi-Motlagh, N., Saberian, M., Li, J., Ranjbar, N., 2021a. Shear strength and life cycle assessment of volcanic ash-based geopolymer and cement stabilized soil: a comparative study. Transp. Geotech. 31, 100639.

Ghadir, P., Miraki, H., Malekahmadi, N., Shariatmadari, N., Javadi, A., 2021b. A comparison on mechanical performance and durability of VA-based geopolymer and Portland cement for soil stabilization. In: Proceeding of the 7th International Young Geotechnical Engineers Conference (in press).

Ghasemi, M., Rasekh, H., Berenjian, J., AzariJafari, H., 2019. Dealing with workability loss challenge in SCC mixtures incorporating natural pozzolans: a study of natural zeolite and pumice. Construct. Build. Mater. 222, 424–436.

Gopalakrishnan, R., Chinnaraju, K., 2019. Durability of ambient cured alumina silicate concrete based on slag/fly ash blends against sulfate environment. Construct. Build. Mater. 204, 70–83.

Hanjitsuwan, S., Hunpratub, S., Thongbai, P., Maensiri, S., Sata, V., Chindaprasirt, P., 2014. Effects of NaOH concentrations on physical and electrical properties of high calcium fly ash geopolymer paste. Cement Concr. Compos. 45, 9–14.

Hardjito, D., Rangan, B.V., 2005. Development and Properties of Low-Calcium Fly Ash-Based Geopolymer Concrete. Reaserch Report. Curtin University of Technology.

Heah, C., Kamarudin, H., Al Bakri, A.M., Bnhussain, M., Luqman, M., Nizar, I.K., Ruzaidi, C., Liew, Y.M., 2012. Study on solids-to-liquid and alkaline activator ratios on kaolin-based geopolymers. Construct. Build. Mater. 35, 912–922.

Higgins, D., 2007. Briefing: GGBS and sustainability. Proc. Inst. Civil Eng.-Const. Mater. 160 (3), 99–101.

Ismail, I., Bernal, S.A., Provis, J.L., San Nicolas, R., Brice, D.G., Kilcullen, A.R., Hamdan, S., van Deventer, J.S., 2013. Influence of fly ash on the water and chloride permeability of alkali-activated slag mortars and concretes. Construct. Build. Mater. 48, 1187–1201.

Ismail, I., Bernal, S.A., Provis, J.L., San Nicolas, R., Hamdan, S., van Deventer, J.S., 2014. Modification of phase evolution in alkali-activated blast furnace slag by the incorporation of fly ash. Cement Concr. Compos. 45, 125–135.

Jahandari, S., Saberian, M., Zivari, F., Li, J., Ghasemi, M., Vali, R., 2017a. Experimental study of the effects of curing time on geotechnical properties of stabilized clay with lime and geogrid. Int. J. Geotech. Eng. 13 (2), 1–12.

Jahandari, S., Li, J., Saberian, M., Shahsavarigoughari, M., 2017b. Experimental study of the effects of geogrids on elasticity modulus, brittleness, strength, and stress-strain behavior of lime stabilized kaolinitic clay. GeoResJ 13, 49–58.

Jahandari, S., Toufigh, M.M., Li, J., Saberian, M., 2017c. Laboratory study of the effect of degrees of saturation on lime concrete resistance due to the groundwater level increment. Geotech. Geol. Eng. 36 (1), 413–424.

Jahandari, S., Saberian, M., Tao, Z., Mojtahedi, S.F., Li, J., Ghasemi, M., Rezvani, S.S., Li, W., 2019. Effects of saturation degrees, freezing thawing, and curing on geotechnical properties of lime and lime-cement concretes. Cold Reg. Sci. Technol. 160, 242–251.

Jahandari, S., Mojtahedi, S.F., Zivari, F., Jafari, M., Mahmoudi, M.R., Shokrgozar, A., Kharazmi, S., Vosough Hosseini, B., Rezvani, S., Jalalifar, H., 2020. The impact of long-term curing period on the mechanical features of lime-geogrid treated soils. Geomechanics Geoengin. https://doi.org/10.1080/17486025.2020.1739753.

Jahandari, S., Tao, Z., Saberian, M., Shariati, M., Li, J., Abolhasani, M., Kazemi, M., Rahmani, A., Rashidi, M., 2021a. Geotechnical properties of lime-geogrid improved clayey subgrade under various moisture conditions. Road Mater. Pavement Des. https://doi.org/10.1080/14680629.2021.1950816.

Jahandari, S., Tao, Z., Alim, M.A., 2021b. Effects of different integral hydrophobic admixtures on the properties of concrete Concrete. In: Proceeding of the Concrete Institute of Australia's 30th Biennial National Conference.

Jiang, J., Yuan, Y., 2013. Relationship of moisture content with temperature and relative humidity in concrete. Mag. Concr. Res. 65 (11), 685–692.

Kaze, C.R., Djobo, J.N.Y., Nana, A., Tchakoute, H.K., Kamseu, E., Melo, U.C., Leonelli, C., Rahier, H., 2018. Effect of silicate modulus on the setting, mechanical strength and microstructure of iron-rich aluminosilicate (laterite) based-geopolymer cured at room temperature. Ceram. Int. 44 (17), 21442–21450.

Kazemi, M., Hajforoush, M., Talebi, P., Daneshfar, M., Shokrgozar, A., Jahandari, S., Saberian, M., Li, J., 2020a. In-situ strength estimation of polypropylene fibre reinforced recycled aggregate concrete using Schmidt rebound hammer and point load test. J. Sustain. Cem.-Based Mater. 1–18.

Kazemi, M., Li, J., Harehdasht, S.L., Yousefieh, N., Jahandari, S., Saberian, M., 2020b. Non-linear behavior of concrete beams reinforced with GFRP and CFRP bars grouted in sleeves. Structures 23, 87–102.

Komnitsas, K., Zaharaki, D., 2007. Geopolymerisation: a review and prospects for the minerals industry. Miner. Eng. 20 (14), 1261–1277.

Kuenzel, C., Vandeperre, L.J., Donatello, S., Boccaccini, A.R., Cheeseman, C., 2012. Ambient temperature drying shrinkage and cracking in metakaolin-based geopolymers. J. Am. Ceram. 95 (10), 3270–3277.

Kupwade-Patil, K., Allouche, E.N., 2013. Impact of alkali silica reaction on fly ash-based geopolymer concrete. J. Mater. Civ. 25 (1), 131–139.

Lemougna, P.N., MacKenzie, K.J., Melo, U.C., 2011. Synthesis and thermal properties of inorganic polymers (geopolymers) for structural and refractory applications from volcanic ash. Ceram. Int. 37 (8), 3011–3018.

Lemougna, P.N., Wang, K.-T., Tang, Q., Melo, U.C., Cui, X.-M., 2016. Recent developments on inorganic polymers synthesis and applications. Ceram. Int. 42 (14), 15142–15159.

Lemougna, P.N., Wang, K.-T., Tang, Q., Cui, X.-M., 2017a. Study on the development of inorganic polymers from red mud and slag system: application in mortar and lightweight materials. Construct. Build. Mater. 156, 486–495.

Lemougna, P.N., Wang, K.-T., Tang, Q., Cui, X.-M., 2017b. Synthesis and characterization of low temperature (< 800 °C) ceramics from red mud geopolymer precursor. Construct. Build. Mater. 131, 564–573.

Lemougna, P.N., Wang, K.-T., Tang, Q., Nzeukou, A., Billong, N., Melo, U.C., Cui, X.-M., 2018. Review on the use of volcanic ashes for engineering applications. Resour. Conserv. Recycl. 137, 177–190.

Lemougna, P.N., Nzeukou, A., Aziwo, B., Tchamba, A., Wang, K.-T., Melo, U.C., Cui, X.-M., 2020. Effect of slag on the improvement of setting time and compressive strength of low reactive volcanic ash geopolymers synthetized at room temperature. Mater. Chem. Phys. 239, 122077.

Lin, D.-F., Lin, K.-L., Hung, M.-J., Luo, H.-L., 2007. Sludge ash/hydrated lime on the geotechnical properties of soft soil. J. Hazard Mater. 145 (1–2), 58–64.

Liu, Z., Cai, C., Liu, F., Fan, F., 2016. Feasibility study of loess stabilization with fly ash-based geopolymer. J. Mater. Civ. 28 (5), 04016003.

Long, G., Gao, Y., Xie, Y., 2015. Designing more sustainable and greener self-compacting concrete. Construct. Build. Mater. 84, 301–306.

Ma, C., Zhao, B., Wang, L., Long, G., Xie, Y., 2020. Clean and low-alkalinity one-part geopolymeric cement: effects of sodium sulfate on microstructure and properties. J. Clean. Prod. 252, 119279.

McLellan, B.C., Williams, R.P., Lay, J., Van Riessen, A., Corder, G.D., 2011. Costs and carbon emissions for geopolymer pastes in comparison to ordinary portland cement. J. Clean. Prod. 19 (9–10), 1080–1090.

Mehdizadeh, B., Jahandari, S., Vessalas, K., Miraki, H., Rasekh, H., Samali, B., 2021. Fresh, mechanical, and durability properties of self-compacting mortar incorporating alumina nanoparticles and rice husk ash. Materials 14 (22), 6778.

Mehrabi, P., Shariati, M., Kabirifar, K., Jarrah, M., Rasekh, H., Trung, N.T., Shariati, A., Jahandari, S., 2021. Effect of pumice powder and nano-clay on the strength and permeability of fiber-reinforced pervious concrete incorporating recycled concrete aggregate. Construct. Build. Mater. 287, 122652.

Mohammadi, M., Kafi, M.A., Kheyroddin, A., Ronagh, H.R., 2019. Experimental and numerical investigation of an innovative buckling-restrained fuse under cyclic loading. Structures 22, 186–199.

Mohammadi, M., Kafi, M.A., Kheyroddin, A., Ronagh, H.R., 2020. Performance of innovative composite buckling-restrained fuse for concentrically braced frames under cyclic loading. Steel Compos. Struct. 36, 163–177.

Nath, P., Sarker, P.K., 2017. Flexural strength and elastic modulus of ambient-cured blended low-calcium fly ash geopolymer concrete. Construct. Build. Mater. 130, 22–31.

Ouyang, X., Ma, Y., Liu, Z., Liang, J., Ye, G., 2020. Effect of the sodium silicate modulus and slag content on fresh and hardened properties of alkali-activated fly ash/slag. Minerals 10 (1), 15.

Pacheco-Torgal, F., Abdollahnejad, Z., Camões, A., Jamshidi, M., Ding, Y., 2012. Durability of alkali-activated binders: a clear advantage over Portland cement or an unproven issue. Construct. Build. Mater. 30, 400–405.

Panagiotopoulou, C., Tsivilis, S., Kakali, G., 2015. Application of the Taguchi approach for the composition optimization of alkali activated fly ash binders. Construct. Build. Mater. 91, 17–22.

Parsajoo, M., Armaghani, D.J., Mohammed, A.S., Khari, M., Jahandari, S., 2021. Tensile strength prediction of rock material using non-destructive tests: a comparative intelligent study. Transp. Geotech. 31, 100652.

Parthiban, K., Saravanarajamohan, K., Shobana, S., Bhaskar, A.A., 2013. Effect of replacement of slag on the mechanical properties of fly ash based geopolymer concrete. Int. J. Eng. Technol. 5 (3), 2555–2559.

PCA, 1992. Soil-cement Laboratory Handbook. Portland Cement Association (PCA), Skokie, IL, USA.

Phetchuay, C., Horpibulsuk, S., Arulrajah, A., Suksiripattanapong, C., Udomchai, A., 2016. Strength development in soft marine clay stabilized by fly ash and calcium carbide residue based geopolymer. Appl. Clay Sci. 127, 134–142.

Phoo-ngernkham, T., Maegawa, A., Mishima, N., Hatanaka, S., Chindaprasirt, P., 2015. Effects of sodium hydroxide and sodium silicate solutions on compressive and shear bond strengths of FA–GBFS geopolymer. Construct. Build. Mater. 91, 1–8.

Phoo-ngernkham, T., Sata, V., Hanjitsuwan, S., Ridtirud, C., Hatanaka, S., Chindaprasirt, P., 2016. Compressive strength, bending and fracture characteristics of high calcium fly ash geopolymer mortar containing portland cement cured at ambient temperature. Arabian J. Sci. Eng. 41 (4), 1263–1271.

Phummiphan, I., Horpibulsuk, S., Sukmak, P., Chinkulkijniwat, A., Arulrajah, A., Shen, S.-L., 2016. Stabilisation of marginal lateritic soil using high calcium fly ash-based geopolymer. Road Mater. Pavement Des. 17 (4), 877–891.

Pourakbar, S., Huat, B.B., Asadi, A., Fasihnikoutalab, M.H., 2016. Model study of alkali-activated waste binder for soil stabilization. Int. J. Geosynth. Ground Eng. 2 (4), 35.

Provis, J.L., Lukey, G.C., Van Deventer, J.S.J., 2005. Do geopolymers actually contain nanocrystalline zeolites? – a reexamination of existing results. Chem. Mater. 17 (12), 3075–3085.

Provis, J.L., Yong, C.Z., Duxson, P., van Deventer, J.S., 2009. Correlating mechanical and thermal properties of sodium silicate-fly ash geopolymers. C Colloids Surf. A Physicochem. Eng. Asp. 336 (1–3), 57–63.

Provis, J.L., Van Deventer, J.S., 2013. Alkali Activated Materials: State-Of-The-Art Report, RILEM TC 224-AAM. Springer Science and Business Media, 98-94.

Provis, J.L., Bernal, S.A., 2014. Geopolymers and related alkali-activated materials. Annu. Rev. Mater. Res. 44, 299–327.

Purnell, P., 2013. The carbon footprint of reinforced concrete. Adv. Concr. Constr. 25 (6), 362–368.

Qiu, J., Zhao, Y., Xing, J., Sun, X., 2019. Fly ash/blast furnace slag-based geopolymer as a potential binder for mine backfilling: effect of binder type and activator concentration. Adv. Mat. Sci. Eng. 2028109, 2019.

Ranjbar, N., Mehrali, M., Alengaram, U.J., Metselaar, H.S.C., Jumaat, M.Z., 2014. Compressive strength and microstructural analysis of fly ash/palm oil fuel ash based geopolymer mortar under elevated temperatures. Construct. Build. Mater. 65, 114–121.

Ranjbar, N., Mehrali, M., Maheri, M.R., Mehrali, M., 2017. Hot-pressed geopolymer. Cement Concr. Res. 100, 14–22.

Rasekh, H., Joshaghani, A., Jahandari, S., Aslani, F., Ghodrat, M., 2020. Rheology and workability of SCC. In: Self-Compacting Concrete: Materials, Properties, and Applications. Elsevier, pp. 31–63.

Rashidian-Dezfouli, H., Rangaraju, P.R., Kothala, V.S.K., 2018. Influence of selected parameters on compressive strength of geopolymer produced from ground glass fiber. Construct. Build. Mater. 162, 393–405.

Rattanasak, U., Chindaprasirt, P., 2009. Influence of NaOH solution on the synthesis of fly ash geopolymer. Miner. Eng. 22 (12), 1073–1078.

Raymon, S., 1961. Pulverized fuel ash as embankment material. Inst. Civ. Eng. Proc. Marit. Eng. 19 (4), 515–536.

Rios, S., Ramos, C., Viana da Fonseca, A., Cruz, N., Rodrigues, C., 2019. Mechanical and durability properties of a soil stabilised with an alkali-activated cement. Eur. J. Environ. Civ. Eng. 23 (2), 245–267.

Robayo-Salazar, R., Mejía-Arcila, J., de Gutiérrez, R.M., Martínez, E., 2018. Life cycle assessment (LCA) of an alkali-activated binary concrete based on natural volcanic pozzolan: a comparative analysis to OPC concrete. Construct. Build. Mater. 176, 103–111.

Saberian, M., Mehrinejad, M., Jahandari, S., Vali, R., Li, J., 2017a. Experimental and phenomenological study of the effects of adding shredded tire chips on geotechnical properties of peat. Int. J. Geotech. Eng. 6362, 1–10.

Saberian, M., Jahandari, S., Li, J., Zivari, F., 2017b. Effect of curing, capillary action, and groundwater level increment on geotechnical properties of lime concrete: experimental and prediction studies. J. Rock Mech. Geotech. Eng. 9 (4), 638–647.

Saberian, M., Mehrinejad Khotbehsara, M., Jahandari, S., Vali, R., Li, J., 2018. Experimental and phenomenological study of the effects of adding shredded tire chips on geotechnical properties of peat. Int. J. Geotech. Eng. 12 (4), 347–356.

Saberian, M., Li, J., Perera, S.T.A.M., Ren, G., Roychand, R., Tokhi, H., 2020. An experimental study on the shear behaviour of recycled concrete aggregate incorporating recycled tyre waste. Construct. Build. Mater. 264, 120266.

Sadeghian, F., Haddad, A., Jahandari, S., Rasekh, H., Ozbakkaloglu, T., 2020. Effects of electrokinetic phenomena on the load-bearing capacity of different steel and concrete piles: a small-scale experimental study. Can. Geotech. J. 58 (5), 741–746.

Sadeghian, F., Jahandari, S., Haddad, A., Rasekh, H., Li, J., 2021. Effects of variations of voltage and pH value on the shear strength of soil and durability of different electrodes and piles during electrokinetic phenomenon. J. Rock Mech. Geotech. Eng. https://doi.org/10.1016/j.jrmge.2021.07.017.

Sadeghi-Nik, A., Bahari, A., Sadeghi-Nik, A., 2011. Investigation of nano structural properties of cement-based materials. Am. J. Sci. Res. 25, 104–111.

Scrivener, K.L., John, V.M., Gartner, E.M., 2018. Eco-efficient cements: potential economically viable solutions for a low-CO_2 cement-based materials industry. Cement Concr. Res. 114, 2–26.

Shand, M.A., 2006. The Chemistry and Technology of Magnesia. John Wiley and Sons.

Shariatmadari, N., Hasanzadehshooiili, H., Ghadir, P., Saeidi, F., Moharami, F., 2021. Compressive strength of sandy soils stabilized with alkali-activated volcanic ash and slag. J. Mater. Civ. Eng. 33 (11), 04021295.

Shi, C., Day, R.L., 2000. Pozzolanic reaction in the presence of chemical activators: Part I. Reaction kinetics. Cement Concr. Res. 30 (1), 51–58.

Shi, Y., Long, G., Ma, C., Xie, Y., He, J., 2019. Design and preparation of ultra-high performance concrete with low environmental impact. J. Clean. Prod. 214, 633–643.

Singhi, B., Laskar, A.I., Ahmed, M.A., 2016. Investigation on soil–geopolymer with slag, fly ash and their blending. Arabian J. Sci. Eng. 41 (2), 393–400.

Singhi, B., Laskar, A.I., Ahmed, M.A., 2017. Mechanical behavior and sulfate resistance of alkali activated stabilized clayey soil. Geotech. Geol. Eng. 35 (5), 1907–1920.

Somna, K., Jaturapitakkul, C., Kajitvichyanukul, P., Chindaprasirt, P., 2011. NaOH-activated ground fly ash geopolymer cured at ambient temperature. Fuel 90 (6), 2118–2124.

Sukmak, P., Sukmak, G., Horpibulsuk, S., Setkit, M., Kassawat, S., Arulrajah, A., 2019. Palm oil fuel ash-soft soil geopolymer for subgrade applications: strength and microstructural evaluation. Road Mater. Pavement Des. 20 (1), 110–131.

Suksiripattanapong, C., Horpibulsuk, S., Chanprasert, P., Sukmak, P., Arulrajah, A., 2015. Compressive strength development in fly ash geopolymer masonry units manufactured from water treatment sludge. Construct. Build. Mater. 82, 20–30.

Takeda, H., Hashimoto, S., Kanie, H., Honda, S., Iwamoto, Y., 2014. Fabrication and characterization of hardened bodies from Japanese volcanic ash using geopolymerization. Ceram. Int. 40 (3), 4071–4076.

Tambara Júnior, L.U.D., Cheriaf, M., Rocha, J.C., 2018. Development of alkaline-activated self-leveling hybrid mortar ash-based composites. Materials 11 (10), 1829.

Tan, J., Cai, J., Li, X., Pan, J., Li, J., 2020. Development of eco-friendly geopolymers with ground mixed recycled aggregates and slag. J. Clean. Prod. 256, 120369.

Tchakouté, H.K., Rüscher, C.H., Kamseu, E., Djobo, J.N., Leonelli, C., 2017. The influence of gibbsite in kaolin and the formation of berlinite on the properties of metakaolin-phosphate-based geopolymer cements. Mater. Chem. Phys. 199, 280–288.

Toghroli, A., Mehrabi, P., Shariati, M., Trung, N.T., Jahandari, S., Rasekh, H., 2020. Evaluating the use of recycled concrete aggregate and pozzolanic additives in fiber-reinforced pervious concrete with industrial and recycled fibers. Construct. Build. Mater. 252, 118997.

Topccedil, I.B., Uygunoğlu, T., 2010. Influence of mineral additive type on slump-flow and yield stress of self-consolidating mortar. Sci. Res. Essays 5 (12), 1492–1500.

Turner, L.K., Collins, F.G., 2013. Carbon dioxide equivalent (CO_2-e) emissions: a comparison between geopolymer and OPC cement concrete. Construct. Build. Mater. 43, 125–130.

Torres-Carrasco, M., Rodríguez-Puertas, C., del Mar Alonso, M., Puertas, F., 2015. Alkali activated slag cements using waste glass as alternative activators. Rheological behaviour. Bol. Soc. Esp. Ceram. V. 54 (2), 45–57.

Van den Heede, P., De Belie, N., 2012. Environmental impact and life cycle assessment (LCA) of traditional and 'green'concretes: literature review and theoretical calculations. Cement Concr. Compos. 34 (4), 431–442.

Van Deventer, J., Provis, J., Duxson, P., Lukey, G., 2007. Reaction mechanisms in the geopolymeric conversion of inorganic waste to useful products. J. Hazard Mater. 139 (3), 506–513.

Verdolotti, L., Iannace, S., Lavorgna, M., Lamanna, R., 2008. Geopolymerization reaction to consolidate incoherent pozzolanic soil. J. Mater. Sci. 43 (3), 865–873.

Wang, S.-D., Scrivener, K.L., 1995. Hydration products of alkali activated slag cement. Cement Concr. Res. 25 (3), 561–571.

Wang, L., 2002. Cementitious Stabilization of Soils in the Presence of Sulfate. PhD Thesis. Louisiana State University and Agricultural and Mechanical College, USA.

Wang, Y., Fall, M., Wu, A., 2016. Initial temperature-dependence of strength development and self-desiccation in cemented paste backfill that contains sodium silicate. Cement Concr. Compos. 67, 101–110.

Xiao, R., Ma, Y., Jiang, X., Zhang, M., Zhang, Y., Wang, Y., Huang, B., He, Q., 2020. Strength, microstructure, efflorescence behavior and environmental impacts of waste glass geopolymers cured at ambient temperature. J. Clean. Prod. 252, 119610.

Xu, H., Van Deventer, J.S., 2002. Geopolymerisation of multiple minerals. Miner. Eng. 15 (12), 1131–1139.

Xu, H., Van Deventer, J.S., 2003. The effect of alkali metals on the formation of geopolymeric gels from alkali-feldspars. Colloids Surf. A Physicochem. Eng. Asp. 216 (1–3), 27–44.

Yaghoubi, M., Arulrajah, A., Disfani, M.M., Horpibulsuk, S., Darmawan, S., Wang, J., 2019. Impact of field conditions on the strength development of a geopolymer stabilized marine clay. Appl. Clay Sci. 167, 33–42.

Yi, Y., Li, C., Liu, S., 2015. Alkali-activated ground-granulated blast furnace slag for stabilization of marine soft clay. J. Mater. Civ. 27 (4), 04014146.

Yip, C.K., Lukey, G.C., Van Deventer, J.S., 2006. Effect of blast furnace slag addition on microstructure and properties of metakaolinite geopolymeric materials. Adv. Cer. Mat. Comp. 153, 187–209.

Yip, C.K., Lukey, G.C., Provis, J.L., Van Deventer, J.S., 2008. Effect of calcium silicate sources on geopolymerisation. Cement Concr. Res. 38 (4), 554–564.

Zannerni, G.M., Fattah, K.P., Al-Tamimi, A.K., 2020. Ambient-cured geopolymer concrete with single alkali activator. Sustain. Mater. Tech. 23, e00131.

Zawrah, M., Farag, R.S., Kohail, M., 2018. Improvement of physical and mechanical properties of geopolymer through addition of zircon. Mater. Chem. Phys. 217, 90–97.

Zhang, Y.S., Sun, W., Li, Z.J., 2010. Composition design and microstructural characterization of calcined kaolin-based geopolymer cement. Appl. Clay Sci. 47 (3–4), 271–275.

Zhang, M., Guo, H., El-Korchi, T., Zhang, G., Tao, M., 2013. Experimental feasibility study of geopolymer as the next-generation soil stabilizer. Construct. Build. Mater. 47, 1468–1478.

Zhao, X., Liu, C., Zuo, L., Wang, L., Zhu, Q., Liu, Y., Zhou, B., 2020. Synthesis and characterization of fly ash geopolymer paste for goaf backfill: reuse of soda residue. J. Clean. Prod. 260, 121045.

Hania Miraki obtained her MSc degree in Civil Engineering from Iran University of Science and Technology which is among the top 5 Universities in Iran. She was ranked within the top 1% at Iran's National University Entrance Exam for Master's degree in Civil Engineering in 2018. She has over 5 years of research experience working in the Laboratory of Soil and Concrete of Abadgaran Negin Jonoobshargh Company (ANJ Co.) on some funded research projects in the areas of concrete durability, soil stabilization, etc. She also has the experience of being teaching assistance at University of Kurdistan, Iran. Hania is currently working as a Research Assistant at Chem Concrete Pty. Ltd. Her research interests include concrete durability, waterproof concrete, geopolymer concrete, soil stabilization and alkali-activated materials. She has recently published a number of high-quality journal publications on the same research topics.